CONTRACTOR REPORT ARSCD-CR-79-007

EXPERIMENTAL PULSED LASER REMOTE CROSSWIND MEASUREMENT SYSTEM — FEASIBILITY STUDY AND DESIGN (PART V)

J. FRED HOLMES
J. RICHARD KERR
RICHARD A. ELLIOTT
MYUNG H. LEE
PHILIP A. PINCUS
MICHAEL E. FOSSEY

DEPARTMENT OF APPLIED PHYSICS & ELECTRONIC SCIENCE
THE OREGON GRADUATE CENTER
19600 N.W. WALKER ROAD
BEAVERTON, OREGON 97005

SEPTEMBER 1978

US ARMY ARMAMENT RESEARCH AND DEVELOPMENT COMMAND
FIRE CONTROL AND SMALL CALIBER WEAPON SYSTEMS LABORATORY
DOVER, NEW JERSEY

NOTICES

Disclaimers

The findings in this report are not to be construed as an official Department of the Army position, unless so designated by other authorized documents.

The citation of trade names and names of manufacturers in this report is not to be construed as official Government indorsement or approval of commercial products or services referenced herein.

Disposition

Destroy this report when it is no longer needed. Do not return it to the originator.

Unclassified

SECURITY CLASSIFICATION OF THIS PAGE *(When Data Entered)*

REPORT DOCUMENTATION PAGE

READ INSTRUCTIONS BEFORE COMPLETING FORM

1 REPORT NUMBER: ARSCD-CR-79-007	2. GOVT ACCESSION NO.
3 RECIPIENT'S CATALOG NUMBER	
4. TITLE *(and Subtitle)*: Experimental Pulsed Laser Remote Crosswind Measurement System Feasibility Study and Design (Part V)	5 TYPE OF REPORT & PERIOD COVERED: Final; 15 November 1976 - 31 December 1977
	6 PERFORMING ORG. REPORT NUMBER: SCF-I-IR(CR)-79-002-FT-5
7. AUTHOR(s): J. Fred Holmes, J. Richard Kerr, Richard A. Elliott, Myung H. Lee, Philip A. Pincus, Michael E. Fossey	8. CONTRACT OR GRANT NUMBER(s): DAAA25-76-C0132
9 PERFORMING ORGANIZATION NAME AND ADDRESS: The Oregon Graduate Center, 19600 N.W. Walker Road, Beaverton, Oregon 97005	10 PROGRAM ELEMENT, PROJECT, TASK AREA & WORK UNIT NUMBERS: 62617A, 1L162617AH19 01, B23G140
11. CONTROLLING OFFICE NAME AND ADDRESS: Commander, ARRADCOM, ATTN: DRDAR-TSS, Dover, NJ 07801	12 REPORT DATE: September 1978 13. NUMBER OF PAGES: 51
14 MONITORING AGENCY NAME & ADDRESS *(if different from Controlling Office)*: Commander, U.S. Army Armament Research and Development Command. Fire Control and Small Caliber Weapon Systems Laboratory, Dover, New Jersey	15 SECURITY CLASS. *(of this report)*: Unclassified 15a DECLASSIFICATION/DOWNGRADING SCHEDULE

16. DISTRIBUTION STATEMENT *(of this Report)*

Approved for public release; distribution unlimited.

17. DISTRIBUTION STATEMENT *(of the abstract entered in Block 20, if different from Report)*

18 SUPPLEMENTARY NOTES

19. KEY WORDS *(Continue on reverse side if necessary and identify by block number)*

Remote Crosswind Measurement, Remote Sensing, Laser Anemometer, Atmospheric Turbulence, Speckle

20. ABSTRACT *(Continue on reverse side if necessary and identify by block number)*

Recent activity with regard to development of a pulsed laser, remote crosswind measurement system is described. Work was concentrated on system improvements and testing. The improvements included the ability to directly measure the average received intensity, a method of aligning the two laser beams so that they are colinear; normalization to compensate for turbulence strength and laser coherence, and accurate automatic gain calibration. Testing included a comparison of the pulsed crosswind system with in situ measurements and cw measurements of the time delayed statistics.

DD FORM 1 JAN 73 1473 EDITION OF 1 NOV 65 IS OBSOLETE

Unclassified

SECURITY CLASSIFICATION OF THIS PAGE *(When Data Entered)*

Experimental Pulsed Laser, Remote Crosswind Measurement System -- Feasibility Study and Design (Part V)

J. Fred Holmes
J. Richard Kerr
Richard A. Elliott
Myung H. Lee
Philip A. Pincus
Michael E. Fossey

Contractor: The Oregon Graduate Center

Sponsor: U.S. Army Armament Research and Development Command
Dover, New Jersey 07801

Contract Number: DAAA25-76-C0132

Effective Date of Contract: 15 November 1976

Contract Expiration Date: 31 December 1977

Principal Investigators: Dr. J. Fred Holmes
Dr. J. Richard Kerr

Project Monitors: Mr. Ira I. Goldberg, U.S. Army Armament Research and Development Command
Dr. Donald L. Walters, U.S. Army Electronics Command
Dr. John M. Zavada, U.S. Army Armament Research and Development Command

TABLE OF CONTENTS

FIGURES

TABLES

INTRODUCTION

In FY 74 Frankford Arsenal through the Atmospheric Sciences Laboratory (ECOM) White Sands Missile Range, New Mexico, initiated a program to develop a remote crosswind measurement system for ballistic applications. A remote crosswind system is needed that will measure the average crosswind between gun and target and automatically feed this data to an onboard ballistics computer for fire control correction of the crosswind error. This error is quite significant, representing one of the largest remaining sources of combat vehicle fire control error, especially with medium and slow muzzle velocity ammunitions (ref. 1).

In an effort to meet this need, a pulsed laser, remote crosswind measurement system is being developed at the Oregon Graduate Center. The present system, although not optimized and fully tested, appears to provide an accurate indication of the path averaged crosswind between the transmitter and target. It still must be demonstrated that the system will work accurately at longer ranges and at low turbulence levels and the limits of accurate system operation must be defined and extended. Work on these tasks and others will be accomplished during the next contract period. The tasks include:

Measurement Pulsed System

- Non-Time Delayed Statistics in Extended Ranges
- Time Delayed Statistics
- Wind Measurement, Variety of Atmospheric Conditions

Equipment and Software Improvement

- Wind Calculation Between Pulse Pairs
- Improved Diode Arrays
- Reduction of Pulse Separation
- Self-adaptive to Signal Strength, Range and Wind
- Error Reduction Through Preprocessing Data and Improved Wind Algorithms

Beam Alignment Effects

- Analytic Formulation
- Definition of Laser Requirements

Coherence Effects

- Analytic Formulation of Partially Coherent Source Problem
- Definition of Laser Requirements

System Optimization

Error Analysis
Numerical Studies

BACKGROUND AND SUMMARY

The feasibility of remotely determining the transverse wind velocity with a point-to-point, cw laser system is well established (refs. 2-4). In more recent work (refs. 5-11), investigators considered the extension of the technique to the use of multiple cw lasers and folded paths as well as ambient light and the use of techniques to overcome saturation. The technique basically consists of relating the scintillation pattern on the receiver to the frozen-in, transverse motion of the turbulence structure along the propagation path. The most successful cw method that has been used involves the measurement of the slope of the log amplitude covariance function at zero time delay (ref. 2).

Using active cw sources, an acceptable signal to noise ratio can be achieved at reasonable transmitter power levels. However, the proposed application of the work sponsored under this project requires a single-ended system operating against a non-cooperative target which can be viewed as a perfectly diffuse surface with reflectivity of approximately 0.1 (ref. 12). Under this constraint, an active cw system would require excessive transmitter power levels.

The primary noise sources in the system are the Poisson fluctuations of a detector current and thermal noise in the electronics. For a given pulse energy, as the pulse width decreases the instantaneous power increases. Consequently, the detector signal current increases and eventually its Poisson fluctuation becomes the dominant noise source. If the receiver is gated synchronously with the transmitted pulses, it can be made signal shot noise limited. Therefore in a direct detection optical system, the signal to noise ratio for a given total energy increases as the pulse duration is made shorter (ref. 13) until the signal shot noise limit is reached. Consequently, a pulsed system can be made considerably more sensitive than a cw system.

In order to employ a pulsed laser and still make a temporal measurement as required for wind velocity, a double-pulse technique has been used (refs. 14, 15, 16) whereby two Q-switched laser pulses are generated at a time interval on the order of a millisecond. This interval appears to be appropriate for the employment of the covariance "slope at zero time lag" technique (ref. 2) and is compatible with current double-pulse laser technology. Initially, a ruby laser was used as a pulsed source.

Since the pulsed technique utilizing a ruby laser precluded time averaging of the statistical quantities measured, spatial averaging had to be employed. Therefore, an array of detectors was used in order to generate a sufficient number of samples of the instantaneous scintillation pattern to use spatial averaging. To the extent that the statistics of this pattern are invariant with lateral translation at the receiver, such spatial averaging will give the desired result; and the pulsed technique is fundamentally similar to the cw, time-averaging approach.

Initially the work on the pulsed laser, remote crosswind measurement system was based on a technique and theory developed for a cw system utilizing a laser directly as a source. This technique and theory, which is based on log-amplitude statistics, has been verified experimentally and is valid for the cw configuration. The basic cw technique is applicable to the pulsed system; however, the detailed theory does not apply to the pulsed configuration. This is not the result of a difference in the propagation characteristics between the pulsed and cw sources, but is caused by the physical differences in the two systems.

The source for the pulsed system is a laser illuminated incoherent target yielding a return path source with an undefined size which at least close to the target gives rise to a temporally coherent, spatially incoherent, Rayleigh distributed field amplitude. This is in contrast to the point source used in the earlier active cw systems and the temporally incoherent cw sources used in later active and passive systems which give rise to log-normal amplitude statistics.

Consequently, the experimental work with the ruby transmitter concentrated largely on tests where the size of the source (at the target) could be controlled (ref. 16). This allowed a better comparison with available theory by decoupling from the experiment the effects of the atmosphere on the laser beam as it propagates from the transmitter to the target. The controlled source size was accomplished by utilizing small disks of scotchlite on a black background as a target.

The results of these tests indicated the need both for a better pulsed source and for a theory applicable to the pulsed system.

A ruby laser was originally chosen as a source because of cost considerations and the realization that energy levels of the order of a joule or greater might be required. Subsequent analysis and experimental results indicated that energy levels of the order of 100 millijoules would yield an adequate signal to noise ratio in the system. Consequently, the system was redesigned to utilize a Nd:YAG laser operating at 1.06 microns. It has the following advantages over the ruby system: much smaller; more rugged; less sensitive to temperature changes; lighter; less power required; much less Radio Frequency Interference (RFI); convection cooled; space-time averaging possible.

Most of the advantages of the Nd:YAG system accrue from the much lower threshold of the lasing medium. Consequently, it requires a much lower input energy per pulse (on the order of 10 in lieu of 1,000 joules). This allows the YAG laser to be double pulsed at a much higher rate than the ruby laser and makes space-time averaging possible. In addition, the lower input energy greatly reduces RFI between the laser and the receiver.

The use of space-time averaging allowed the size of the optical receiver array (spatial averaging) to be reduced from 64 elements (8 × 8) to 16 elements (2 × 8). The laser can produce a double pulse once every 100 milliseconds, and the number of double pulses used for a crosswind measurement can be adjusted from one to forty. An additional advantage of the time averaging is that it tends to eliminate any intermittency of turbulence problems. The YAG system was constructed and at the start of the present report period was ready for verification tests and debugging. This phase of the development required almost 10 months and consisted of system problem identification and solution. Some of the problems encountered and solved were: the need to directly measure the average received intensity as opposed to calculating it; the need for an effective method of aligning the two laser beams in the transmitter so that they are colinear; the need for a method of normalization to compensate for turbulence strength and laser coherence; noise and crosstalk in the receiver; the need for an adjustable time delay between pulses; and the need for accurate, automatic gain calibration of the 16 receiver channels. The pulsed wind sensor is now fully operational and is providing significant data with which to evaluate and optimize the overall system.

Since a theory applicable to the pulsed system was not available, a new theoretical formulation for the statistics of the received intensity based on the extended Huygens-Fresnel principle was developed (refs. 16-18). Our first theoretical effort invoked the assumption of Gaussian field statistics at the receiver. Because of this assumption, only phase perturbation effects, which show up as a dependence on the transverse correlation scale (ρ_o), which appear in the result. This was initially thought to be a good assumption, at least for low turbulence levels, on the basis that the relation between the two turbulence scale sizes (ρ_o and $\sqrt{L/k}$) was expected to be multiplicative and, therefore, the smaller scale - which is usually ρ_o in the present application - would be dominant.

Our cw experiments (ref. 17) confirmed that at low turbulence levels, the Gaussian assumption is indeed correct for the variance and covariance. However, at intermediate turbulence levels the scale size approaches $\sqrt{L/k}$. This suggested that the log-amplitude term, which is responsible for this scale size, plays an important part in the statistics of the received intensity and particularly with regard to remote wind sensing.

Consequently, a complete theoretical formulation including the log-amplitude term was developed (ref. 17). It shows that the relationship between the two scale sizes is additive rather than multiplicative as indicated by the cw experimental data. This means that $\sqrt{L/k}$ scale size can be dominant for our application and that the same mechanism which has been used as a basis for the successful cw wind sensing work performed by NOAA is available for utilization by the pulsed, diffuse-target case.

During the present contract period, additional data was obtained from our cw experiments to increase our confidence in the complete theoretical formulations. In addition, the cw experimental site was relocated adjacent to the pulsed experimental facility. This required a major effort including constructing a new building, and moving and realigning the cw equipment. The reason for this action was to provide a propagation path for the cw experiment where the wind is primarily across the path. This is needed in order to measure the time-delayed statistics for comparison with the theory. These measurements have been completed and good qualitative agreement with the theory was obtained.

Analytic work during the present contract period was concentrated on numerical work in support of the pulsed and the cw experimental efforts. Specifically, more efficient techniques were developed for obtaining numbers from the theoretical formulations which included algorithms for evaluating the two source wave structure function and two source log-amplitude covariance function.

SYSTEM CONSIDERATION

Several new techniques were developed for improving system performance during the contract period. These included: finding a method of aligning the laser beams; adding hardware and software for direct average measurements; introducing a time delay between when the laser starts pulsing and when data is taken; and gain leveling.

The two laser beams used in the transmitter must be colinear in order to measure the time delayed statistics and hence the crosswind. Initially, the beams were aligned by observing them with an infrared viewer at the target and adjusting the transmitter until the spots overlap. This was difficult and highly inconvenient because the target spots could be resolved only during very low turbulence and ambient light conditions, and the observer and adjuster were physically separated by 500 meters.

In order to overcome this problem, a method of checking and adjusting beam alignment within the confines of the field site building was developed. The method involves frequency doubling the 1.06 micron radiation from the transmitter to obtain visible light (green) and then projecting the far field pattern on a screen. The arrangement is

illustrated in figure 1.

A secondary benefit of converting to visible light for alignment was the discovery that during the first few seconds of operation, the laser beam is highly distorted. We are now compensating for this by using a longer burst of pulses and ignoring the data for the first 2 seconds. A noticeable improvement was achieved.

Because the laser used in the system is temporally quite incoherent, the atmospherically induced fluctuations in received intensity which carry the wind information are only a fraction of the mean value of received intensity. Consequently, the mean value must be measured with a high degree of precision in order not to create a large error in the crosswind measurement. This requires that an aperture averaged measurement of the mean intensity be made and that careful attention be paid to gain-leveling the sixteen receiver channels.

We had anticipated that averaging the sixteen receiver channels might not yield a mean intensity measurement of sufficient accuracy; and consequently had made provision for adding a beam splitter and mean value receiver in the optical train. Our subsequent experimental work confirmed the need for a direct average measurement. However, when we tried to implement the beam splitter technique, our efforts were frustrated by the fact that the laser had been designed such that the two pulses were orthogonally polarized.

With a perfectly diffuse target, the return should be randomly polarized and independent of the polarization of the incident beam. In practice, it was found that real, diffuse like targets retain some of the polarization of the incident beam. This coupled with a polarization sensitive beam splitter, convinced us to terminate the beam splitter approach and to build a small separate receiver to monitor the mean intensity from each pulse. In a field version of the system, the beam splitter approach should be used to save space. Consequently, the next version of the laser transmitter should either be circularly polarized or have both pulses linearly polarized in the same direction.

Gain leveling of the receivers is done automatically by the processor. In order to gain level the receivers, a uniform intensity is required to be incident on the receiver optics. This is accomplished by illuminating a target some distance from the receiver with the laser transmitter. The received intensity for any particular pulse will vary from detector to detector due to turbulence. However, on the average it will be the same value. Consequently, by taking many samples (600 presently) and averaging, the relative gain of each of the sixteen channels and the average receiver is determined. Separate gain constants for each of the two pulses in a pulse pair are determined and stored by the computer. This procedure yields a gain leveling good to about one percent which appears to be adequate for the application. Best results are obtained when one of the center

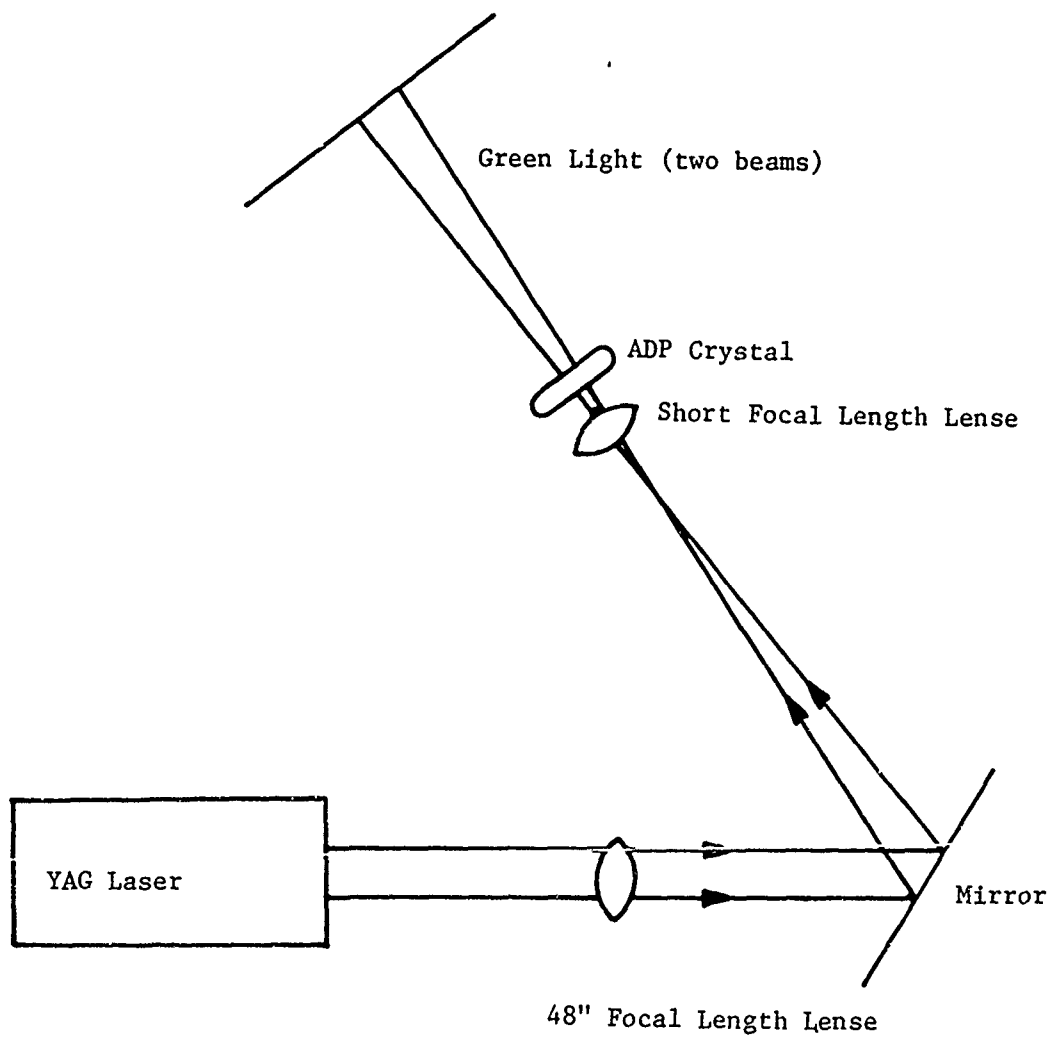

Figure 1. Beam alignment setup.

most elements in the receiver array are used as a reference.

LASER BEAM ALIGNMENT

In order to measure the time delayed covariance from which the crosswind is derived, two laser pulses separated in time must be used. However, if the laser beams are misaligned, they do not travel through the same portion of the atmosphere. Consequently, the atmospherically induced fluctuations on the received intensity from the two pulses separated in time that make up a measurement pair become decorrelated. Since it is the correlated fluctuations that contain the wind information, misalignment of the beams degrades and/or prevents proper system operation.

A good measure of the degree of correlation can be obtained by observing the autocovariance function defined by

$$C_{I_N}(\bar{r},\tau)\Big|_{\bar{r}=0} = \frac{\langle\left(I(\bar{r}_2,t_2) - \bar{I}\right)\left(I(\bar{r}_1,t_1) - \bar{I}\right)\rangle}{\sigma_I^2}$$

where $t_2 - t_1 = \tau$ = time delay between pulses

$\bar{r} = \bar{r}_2 - \bar{r}_1$ = separation between detectors

and σ_I^2 is the variance

This quantity can be thought of as being proportional to the signal we are trying to measure. Consequently, if it is reduced by beam misalignment, this is equivalent to reducing the signal to noise ratio of the system and thereby increasing the wind measurement error. In addition, as the beams separate, the system calibration constant changes. This introduces additional measurement error.

Figure 2 shows the results of some measurements at 1582 meters. The data were obtained by misaligning the beams by a set amount and then measuring the autocovariance. As predicted, it does fall off significantly as the beams separate. If a drop of 10% in the autocovariance can be tolerated, then the data indicate that the beam misalignment on a pulse to pulse basis must be no worse than the laser beam divergence/3.

The actual requirement probably depends on range, transmitter size and turbulence level. The beams must physically overlap to some as yet unknown degree in order for the fluctuations to be correlated sufficiently by the atmosphere. Qualitatively then it would seem that with the atmospheric fluctuations dominant (as opposed to speckle), there are two regimes with respect to the effect of range and turbulence on the error caused by beam misalignment:

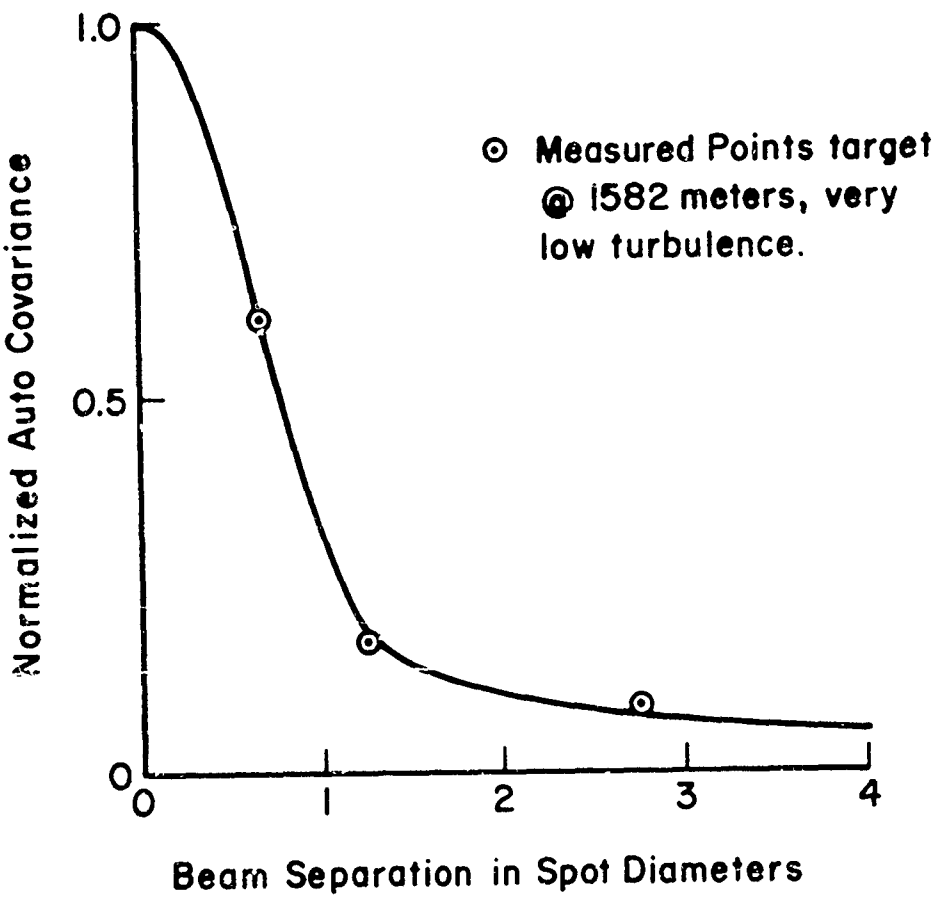

Figure 2. Autocovariance versus beam separation.

The beam spread due to laser coherence and the turbulence is (1) greater than the beam misalignment or (2) less than the beam misalignment. In the first case the sensitivity of the system and the accuracy should increase with turbulence level and range and in the latter case decrease.

Our operational experience to date has fallen into the second regime; however, it would be much more desirable to operate in the first regime. Changes to the laser transmitter would make this possible.

In the second regime, due to the dependence of the calibration constant on beam alignment, the fluctuations in indicated crosswind should increase with range thereby giving an increasing RMS error with range. This has been our experience to date and is the opposite of what was expected prior to encountering the beam alignment problem. With perfectly aligned beams, it is expected that the error will decrease with range (neglecting S/N limitations) due to increased path averaging and increased integrated path turbulence. There may be a limit as to how far in range this argument might be valid due to saturation effects; however, we have not yet encountered anything experientially that could be reasonably attributed to saturation.

Another deleterious effect of beam misalignment is that it increases the lower limit of turbulence level at which the system will operate. As the turbulence level decreases, a point will be reached at which the speckle field will start to dominate (see the section on laser coherence) and the system will lose its sensitivity to the crosswind. If the beams are misaligned, this will occur prematurely since the misalignment desensitizes the system to the atmospherically induced fluctuations that carry the wind information.

Also, it appears that a horizontal misalignment of the beams will cause a constant bias to the indicated wind. The system responds to the shifting of the scintillation pattern with the wind. If the beam for the second pulse is displaced horizontally from the beam for the first pulse, then the pattern will appear to the system to have shifted even if there is no wind. Consequently, if data for the wind measured by the pulsed system were plotted versus the actual wind, the plot would not pass through the origin. This would represent a constant error and the system would indicate a wind when in fact there was no wind. This has been observed experimentally at the Oregon Graduate Center test site.

The beam misalignment in the present transmitter can be separated into two parts: (1) a mechanical slowly varying misalignment; and (2) a pulse to pulse jitter. The mechanical misalignment can be reduced to an acceptable level on a short term basis as discussed in a section on System Consideration by adjusting a steering mirror for one of the beams to make them colinear. Changes in ambient temperature and/or shock and vibration will bring the beams out of alignment. Typically,

the beams will drift several spot diameters apart overnight and seem to be in a continuous process of drifting in and out of alignment during operation of the system.

The pulse to pulse jitter in the present laser transmitter is of the order of a spot diameter. It cannot be reduced with the present laser by adjustment. Reduction of pulse to pulse jitter will require a different approach to the laser design. Based on the results of figure 3 and our operating experience, it appears that a laser beam alignment and RMS jitter specification of around one-tenth the beam divergence should allow good system operation. A more definitive specification will be available after the analytic work on the beam alignment problem is completed.

LASER COHERENCE

A spatially incoherent but temporarily coherent source gives rise to a vacuum speckle of unity contrast ratio. This can represent a strong source of noise in such applications as remote sensing, optical radar, coherent imaging and COAT systems or it can be the signal itself as in speckle interferometry. When these applications involve propagation through the atmosphere, the interaction of the speckle field with the turbulent atmosphere can change its character. Consequently, an understanding of the interaction of the speckle field with the atmosphere is necessary.

There are nine combinations of spatial and temporal coherence of the source as indicated in table 1. The strongest speckle field, of course, occurs for a temporarily coherent but spatially incoherent source. As the spatial coherence increases and/or the temporal coherence decreases, the vacuum contrast ratio decreases from unity and approaches zero as the source either becomes spatially coherent or temporarily incoherent as shown in figure 4. Consequently, only four of the regimes shown in table 1 exhibit speckle.

There are two common physical configurations with regard to speckle field propagation through the turbulent atmosphere. They are the double ended configuration, such as with speckle interferometry, where the transmitter is at one end of the propagation path and the receiver is at the other, and the single ended configuration, which applies to the remote sensing, optical radar, coherent imaging and COAT system application, where the transmitter and receiver are at the same end of the path. In the latter case, the effect of the atmosphere on the transmitted energy must be evaluated both for the propagation from the transmitter to the target and for the propagation from the target back to the receiver. If a temporally and spatially coherent source is used, then the speckle field source is the energy scattered from the target. Consequently, the spatial coherence for the return trip propagation is determined by the target, with a mirror or retroreflector yielding a spatially coherent source, a perfectly

Table 1. Speckle regimes.

Temporal Coherence → / Spatial Coherence ↓	Coherent	Partially Coherent	Incoherent
Coherent	No Speckle	No Speckle	No Speckle
Partially Coherent	Some results available Work in Progress	Work in Progress	No Speckle
Incoherent	Work Completed	Work in Progress	No Speckle

diffuse target yielding a spatially incoherent source and with most real targets falling somewhere in between and giving both specular and diffuse scattering. The specular part is usually referred to as glint and plays an important role in COAT systems.

Past work at the Oregon Graduate Center on speckle propagation through the turbulent atmosphere has been concentrated primarily on the case of a temporally and spatially coherent transmitter used in conjunction with a perfectly diffuse target. Analytic formulations have been developed (refs. 17 and 18) for the first and second order statistics of the intensity. In addition, the variance and covariance of the intensity have been measured experimentally (ref. 19) and excellent quantitative agreement was obtained with the theory for the covariance and a good qualitative agreement was obtained with the analytic results for the variance.

It was found that three scale sizes are important to the covariance. They are the speckle scale size which, of course, depends on the transmitter spot size on the target, the atmosphere phase perturbation scale size ρ_o and the atmosphere log-amplitude perturbation scale size $\sqrt{L/k}$. At very low turbulence levels, the speckle scale size is dominant and at very high turbulence levels ρ_o is dominant. In between, any of the scale sizes may be dominant depending on their relative size and the integrated path turbulence.

There is a simplified theory available (ref. 17) for low turbulence that is useful for some problems. It has also been shown analytically (ref. 17) and experimentally (ref. 19) that the intensity statistics are exponential at low turbulence levels.

The normalized variance for this regime is unity at very low turbulence; and as the turbulence increases, it rises above unity until it reaches a peak value of around 1.25. As turbulence further increases, the normalized variance decreases until it again reaches unity as shown in figure 3.

When the transmitted beam is scattered by the target, the phase of the scattered field is completely randomized. Consequently, the phase perturbation caused by the atmosphere cannot further increase the variance. However, the log-amplitude perturbation is not so constrained and accounts for the increase of the normalized variance above unity. As the turbulence increases, the log-amplitude perturbation eventually saturates and the atmospheric perturbation becomes dominated by the phase perturbation. Consequently, the normalized variance returns to unity at high turbulence levels.

Work on the temporally coherent, spatially incoherent regime is considered to be substantially complete. No new work in this regime is being contemplated at this time by the Oregon Graduate Center. However, for reasons discussed below, of most importance to the remote crosswind measurement system is the temporally and spatially, partially

coherent regime. Work is in process on this important problem.

For the remote crosswind measurement system, the fluctuations in the received intensity are caused both by the speckle and by the atmospheric turbulence. The speckle dominates at low turbulence and the atmosphere dominates at higher turbulence levels. The transition occurs at a turbulence level that decreases as the temporal coherence of the laser decreases.

The transition to domination by speckle can be observed by monitoring the normalized autocovariance function. The fields from the transmitter laser pulses are not correlated to any great degree (if at all) on a pulse to pulse basis. Consequently, in the absence of turbulence, the autocovariance is near zero. As the turbulence increases, the autocovariance will increase due to the common atmospheric turbulence through which the laser pulses propagate until the turbulence dominates the speckle. This is illustrated qualitatively in figure 4 and has been observed experimentally with the pulsed system.

The speckle fields of course carry no information about the crosswind. Consequently, for a given target range there will be a turbulence level below which the system will not respond to a crosswind. The turbulence level at which this occurs decreases with decreasing laser coherence. It also is affected by beam misalignment (see section on Laser Beam Alignment). Fortunately, the laser used in the system has a low coherence which minimizes the effect on system operation. Also, at longer target ranges it should be less of a problem. It should also be noted that as the speckle fields become dominant, the indicated crosswind velocity will drop towards zero and therefore will not make the fire control solution any worse than it would be without the crosswind correction. However, the transition point should be made as low as possible to enhance the utility of the system. Also, it should be noted that the autocovariance can be used as an indicator of whether or not the system is accurately measuring the wind.

The availability of low turbulence data has allowed us to gain some insight into the relationship between the normalized variance and the turbulence strength for the partially coherent transmitter used in the system. The variance is an important parameter in that it is used to normalize the measured statistics that are used to estimate the crosswind. Normalization is required to make the wind calibration constant independent of turbulence level.

The use of the variance for normalization implies that it is proportional to the strength of turbulence C_n^2. Figure 3 shows qualitatively the relationship between the normalized variance and the strength of turbulence for three degrees of coherence. The perfectly coherent source, diffuse target problem has been solved analytically and the analysis has been verified by experimental work as indicated above. Consequently, the relationship shown in figure 3 for the

perfectly coherent source is correct.

The partially coherent source, diffuse target problem has not been solved analytically; and so, the relationships shown in figure 3 for this case are partly conjecture and partly based on our pulsed experimental work. For the limiting case of the incoherent source, there is no residual variance due to speckle; and so the variance must be zero in the absence of turbulence. In addition, there are theoretical reasons to believe that for the incoherent case the variance and the turbulence have a linear relationship until saturation occurs. Consequently, the variance should be proportional to the strength of turbulence for this case.

If the laser source were perfectly incoherent, then normalizing by the variance would compensate for the strength of turbulence. However, the laser source used in the system is partially coherent and consequently, as shown in figure 3 there will be a residual variance at zero turbulence due to the speckle field. This does complicate the problem somewhat, but fortunately the relationship appears to still be linear. However, our pulsed experimental work to date indicates that the relationship is linear with respect to C_n and not C_n^2.

In summary then, it appears that the temporal coherence of the laser transmitter used in the system should be: (1) as low as possible in order to lower the minimum turbulence level at which the system will accurately measure the wind, and (2) should remain constant in order to allow the system to be normalized with respect to turbulence level.

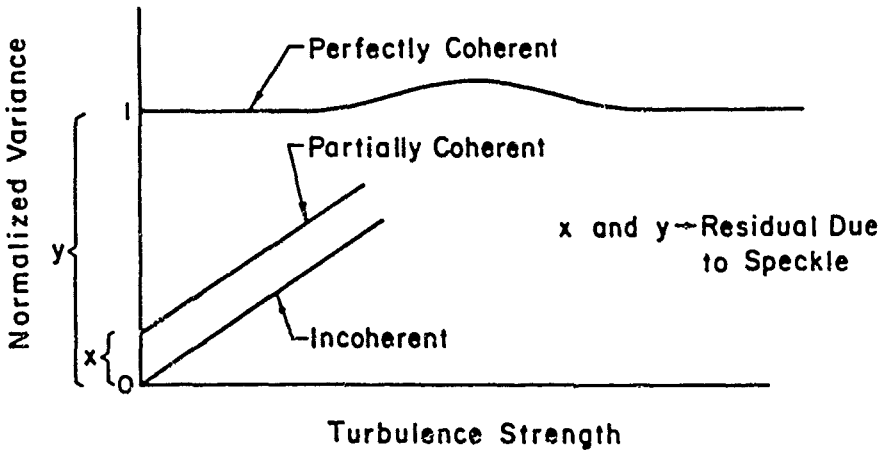

Figure 3. Relationship of the variance to turbulence strength for different values of laser temporal coherence.

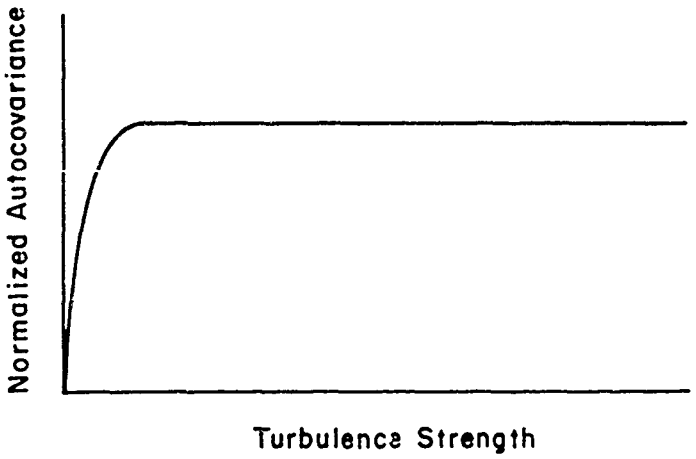

Figure 4. Transition of autocovariance at low turbulence levels.

PULSED EXPERIMENTAL WORK

Variance data that we have collected with a focused transmitter and with a target at 500 meters is shown in figure 5 for pulse #1 and in figure 6 for pulse #2. Each curve represents 12,200 shots taken in forty shot bursts (4 seconds). Data obtained for the same turbulence level were averaged before plotting. However, the linear regression analysis to obtain the best straight line fit and the RMS error calculation were performed on the data before averaging. The data does indicate a linear relationship which has very positive implications with regard to the design of a pulsed laser remote wind sensing system. It also should allow the system to remotely sense the turbulence level which may have some impact with respect to characterizing the electro-optic environment.

The linear fit to the data yields almost identical equations for each pulse. This indicates that at least on the average, both lasers in the transmitter had nearly the same degree of coherence. The RMS errors for each pulse are different however. This implies that the degree of coherence fluctuation is different for the two lasers. It is important that both lasers have nearly the same degree of coherence and that the degree of coherence is stable. This will have to be taken into account in future transmitter designs.

An analytic solution to the partially coherent source, diffuse target problem is needed. It has been proposed as a task for the next contract period.

Covariance data versus turbulence strength for a focused transmitter with a target at 500 meters is shown in figures 7 and 8. A theoretical curve is also shown based on our earlier work on the perfectly coherent source. Although, the actual source used was only partially coherent, it is expected that the trend with increasing turbulence level should be the same. As expected, the covariance both for the data and the theoretical curve falls off with increasing turbulence level indicating a decrease in scale size. The covariance does have an effect on both error and calibration and is a function of range as well as turbulence level. However, it can be controlled by changing the apparent detector spacing.

Crosswind data taken during the contract period is shown in figures 9 through 13 as time series. In addition, the data corresponding to the data plots is given in tables 2 through 6. In all cases, the target is located 500 meters from the transmitter. The curves and data labelled Campbell unit represent the wind as measured by a commercial, cw laser anemometer. It is a space averaging anemometer and has an accuracy of ± 0.5 meter/second. The path weighting function for the Campbell unit is not the same as for the pulsed system. Consequently, part of the difference in their readings may be attributed to this, which is particularly true during low, changing, or

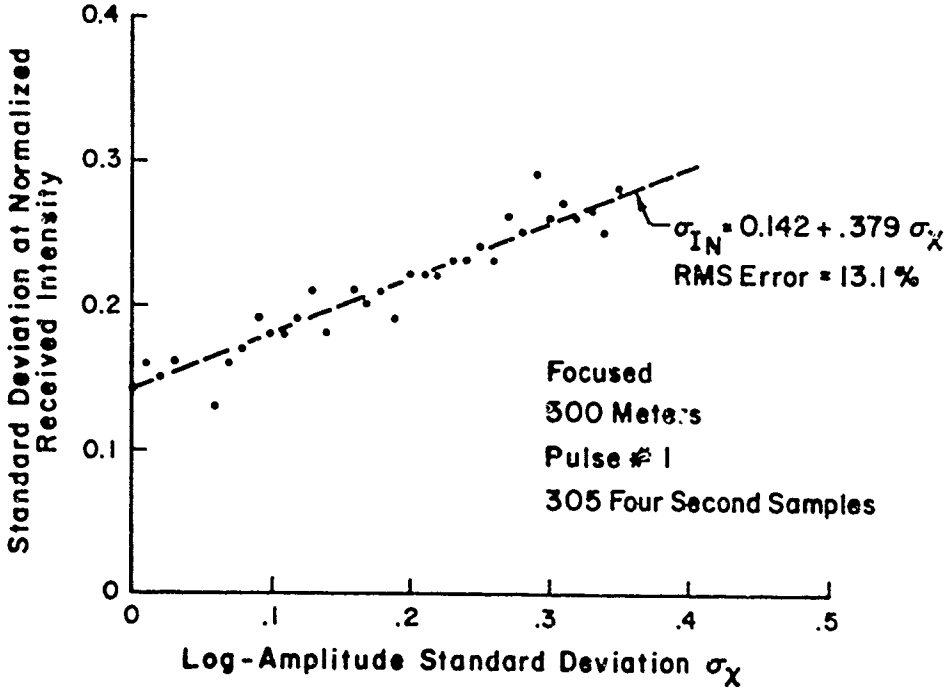

Figure 5. Standard deviation of normalized received intensity versus σ_χ for Pulse #1.

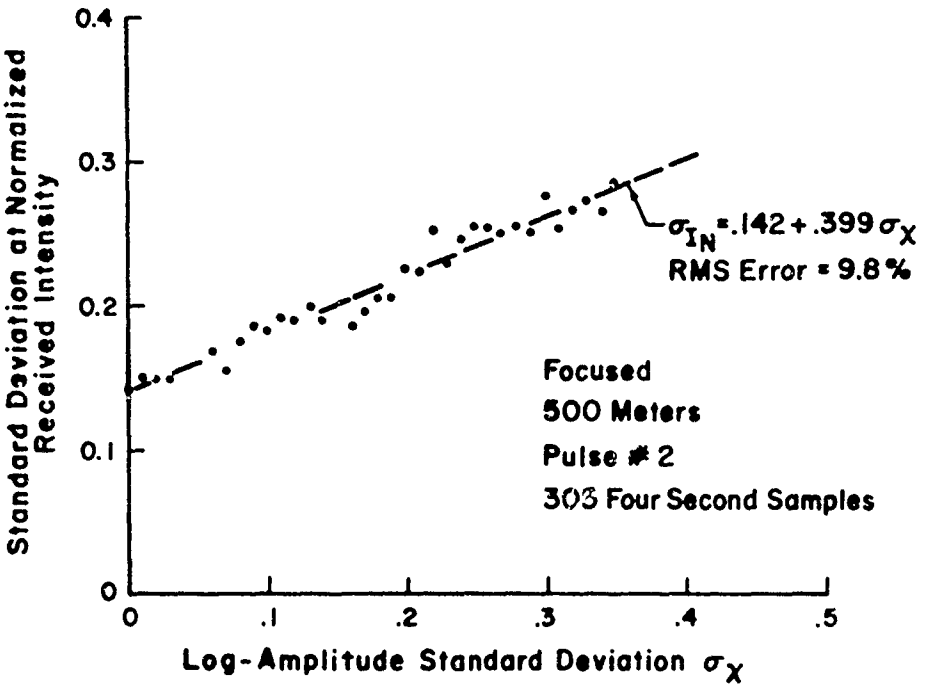

Figure 6. Standard deviation of normalized received intensity versus σ_χ for Pulse #2.

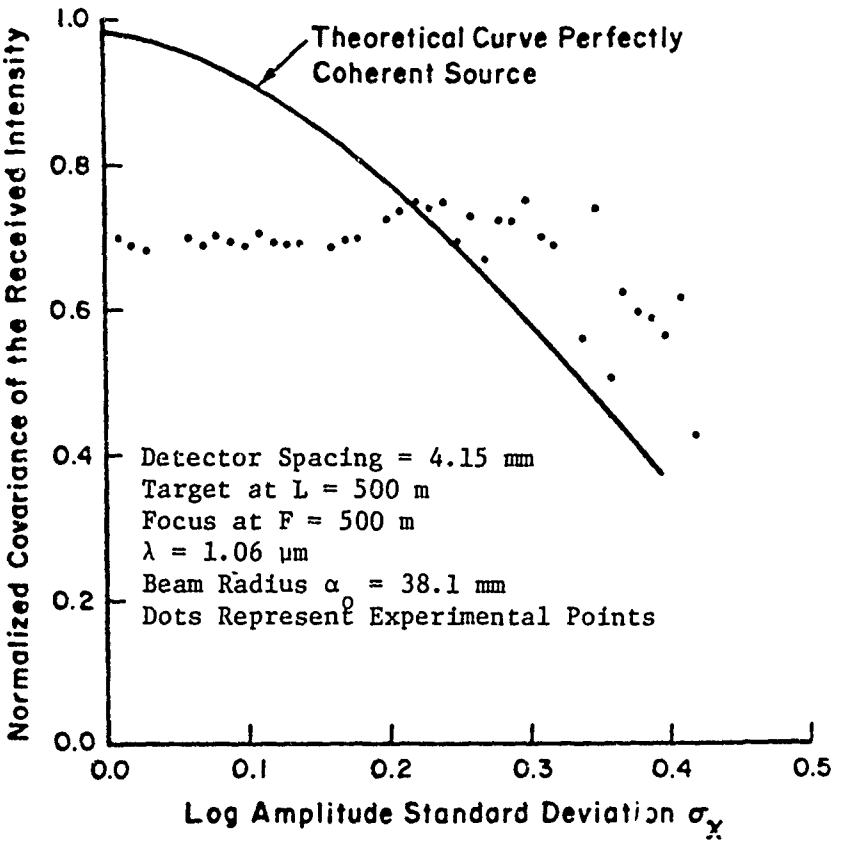

Figure 7. Covariance, focused.

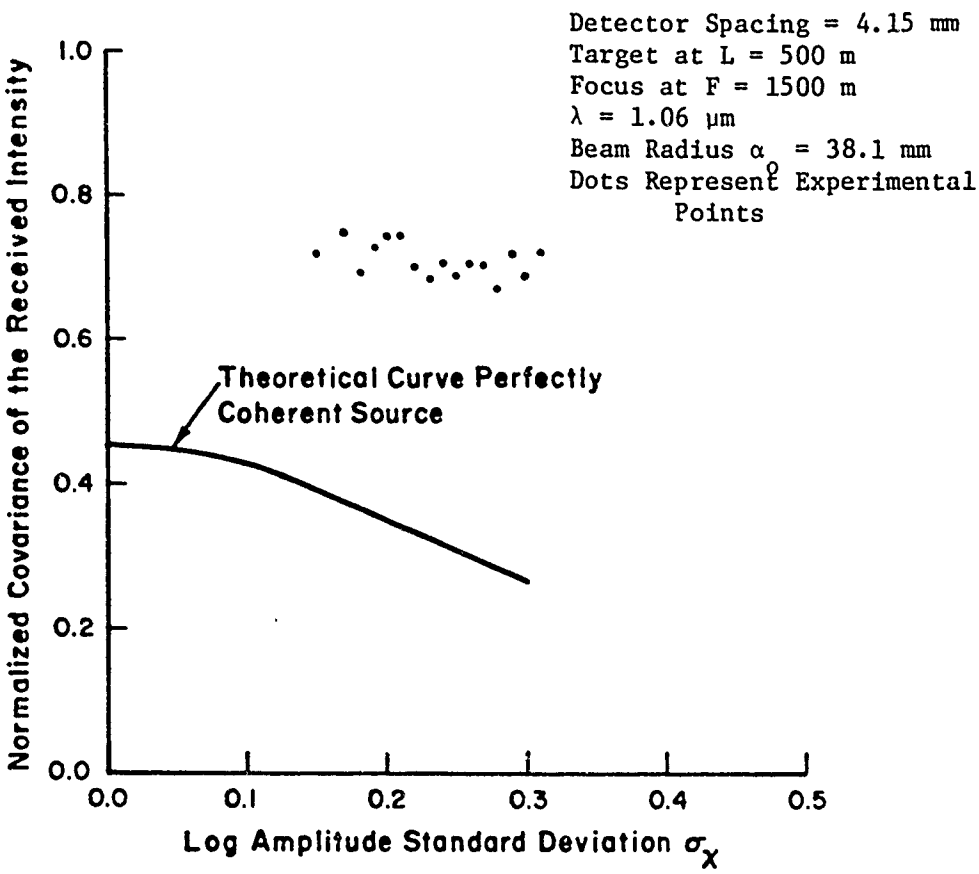

Figure 8. Covariance, defocused.

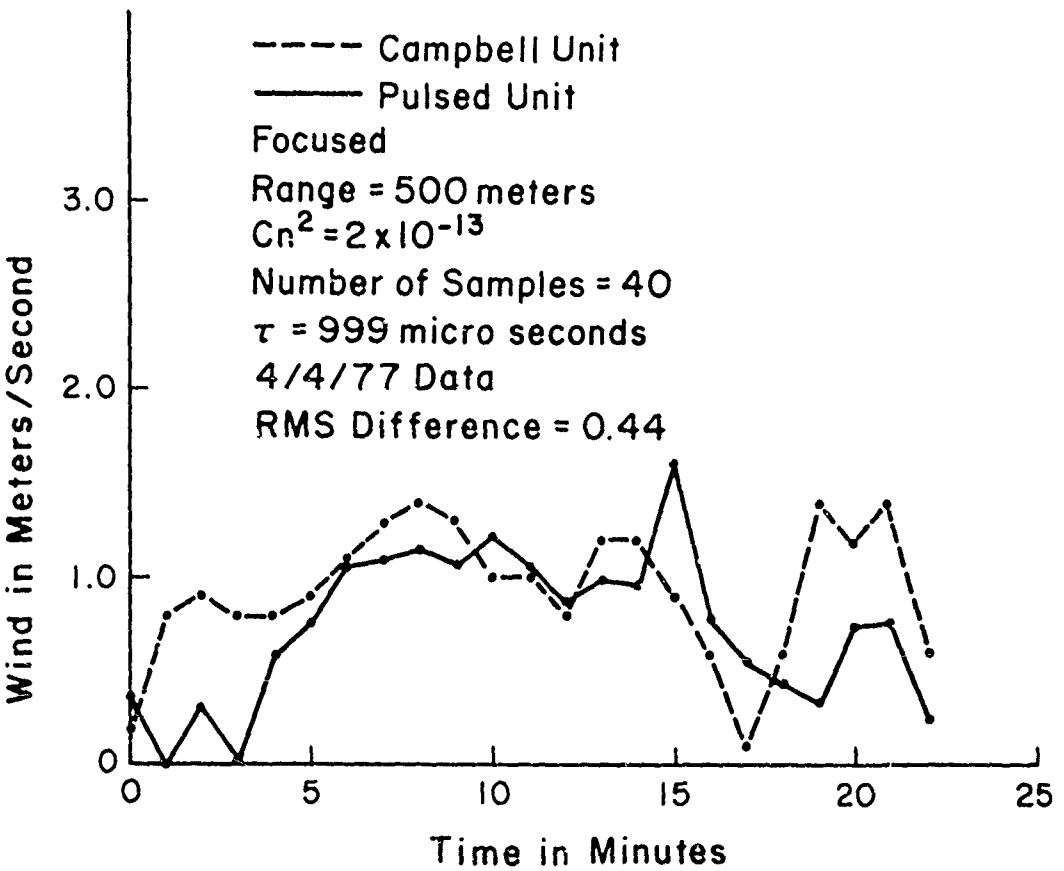

Figure 9. Crosswind, $C_n^2 = 2 \times 10^{-13}$.

Table 2. Crosswind data, $C_n^2 = 2 \times 10^{-13}$.

Oregon Graduate Center

Range = 500 meters
Time Between Pulses = 999 microseconds
Number of Samples = 40
$C_n^2 \simeq 2 \times 10^{-13}$

Campbell	Slope	Pulsed*	Difference
0.2	24	0.39	0.19
0.8	-5	-0.08	-0.88
0.9	19	0.31	-0.59
0.8	2	0.03	-0.77
0.8	37	0.6	-0.2
0.9	48	0.77	-0.13
1.1	68	1.09	-0.01
1.3	69	1.11	-0.19
1.4	71	1.14	-0.26
1.3	67	1.08	-0.22
1.0	75	1.21	+0.21
1.0	65	1.05	+0.05
0.8	54	0.87	+0.07
1.2	63	1.0	-0.20
1.2	61	0.98	-0.22
0.9	101	1.62	+0.72
0.6	48	0.77	+0.17
0.1	35	0.56	+0.46
0.6	28	0.45	-0.15
1.4	22	0.35	-1.05
1.2	46	0.74	-0.46
1.4	48	0.77	-0.63
0.6	15	0.24	-0.36

RMS Difference = .435

*Using calibration constant that minimizes the error = 0.0161
Focused with 1" transmitter stop

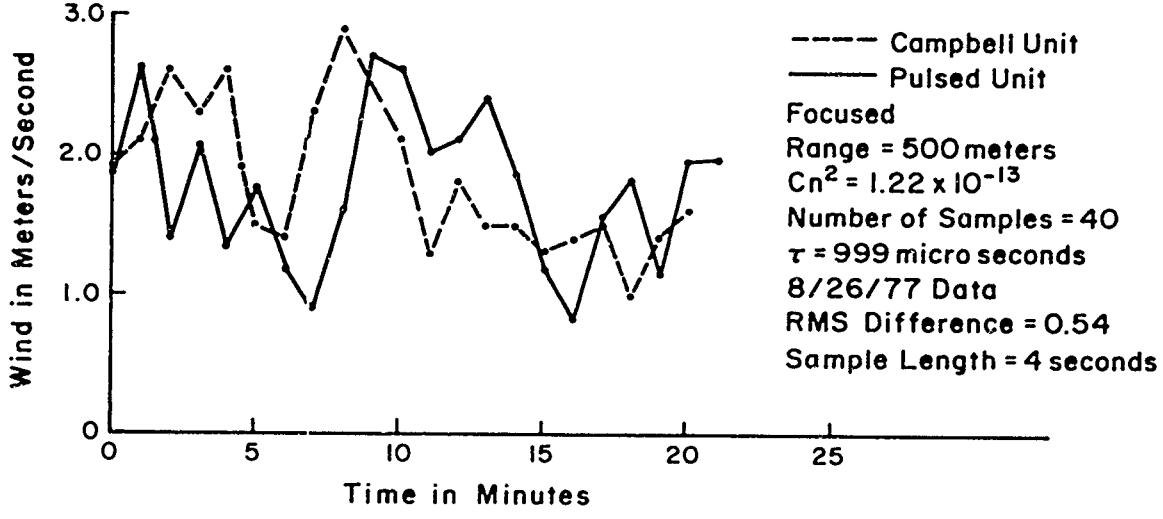

Figure 10. Crosswind, $C_n^2 = 1.22 \times 10^{-13}$.

Table 3. Crosswind data, $C_n^2 = 1.22 \times 10^{-13}$.

Oregon Graduate Center

Range = 500 meters
Time Between Pulses = 999 microseconds
Number of Samples = 40
$C_n^2 = 1.22 \times 10^{-13}$

Focused Beam Campbell	Slope	Pulsed*
1.9	86	1.88
2.1	120	2.62
2.6	63	1.38
2.3	94	2.06
2.6	61	1.33
1.9	80	1.75
1.5	54	1.18
1.4	41	0.9
2.3	72	1.6
2.9	123	2.70
2.7	119	2.60
2.1	92	2.01
1.3	96	2.10
1.8	110	2.40
1.5	84	1.84
1.5	55	1.20
1.3	38	0.83
1.4	71	1.55
1.5	83	1.82
1.0	53	1.16
1.4	89	1.95
1.6	90	1.97

RMS Difference = 0.54 meters per second

*Using calibration constant = 0.02186

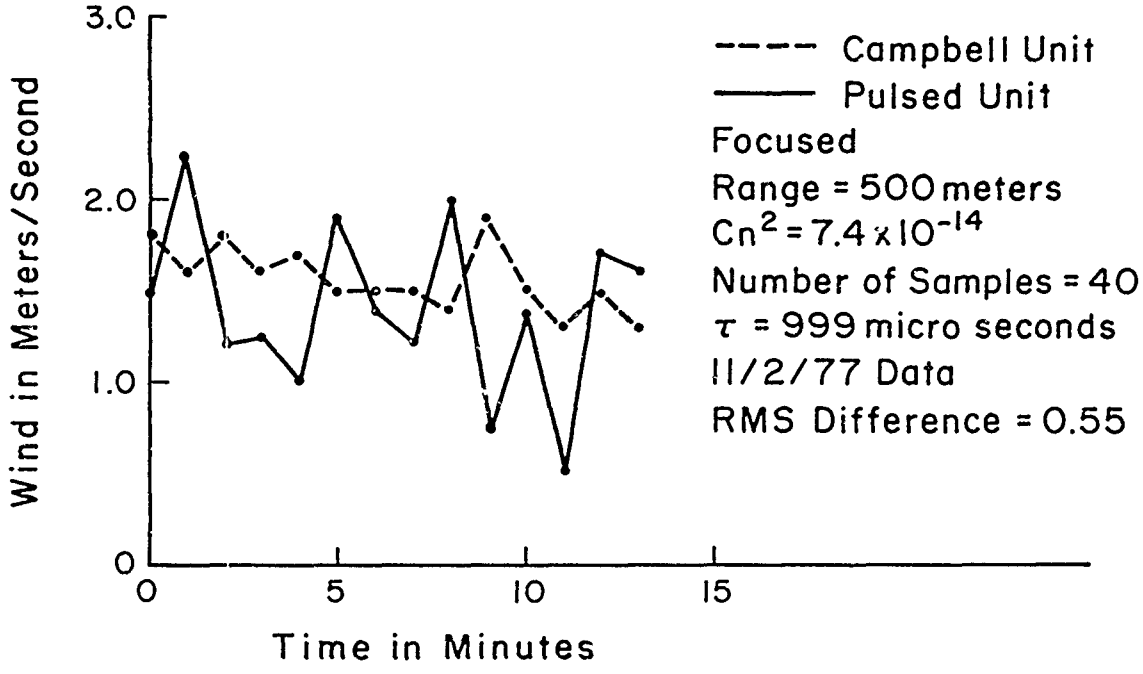

Figure 11. Crosswind, $C_n^2 = 7.4 \times 10^{-14}$.

Table 4. Crosswind data, $C_n^2 = 7.4 \times 10^{-14}$.

Oregon Graduate Center

Range = 500 meters
Time Between Pulses = 999 microseconds
Number of Samples = 40
$C_n^2 = 7.4 \times 10^{-14}$

Campbell	Slope	Pulsed*
1.8	114	1.51
1.6	171	2.26
1.8	91	1.2
1.6	95	1.26
1.7	75	0.99
1.5	144	1.91
1.5	105	1.39
1.5	93	1.23
1.4	150	1.99
1.9	57	0.75
1.6	105	1.39
1.3	40	0.53
1.5	130	1.72
1.3	122	1.62

$\overline{W^2} = 2.50$

$\overline{S^2}$ 12,553

$\overline{WS} = 166$

RMS Difference = 0.55

*Using Calibration Constant = 0.01324

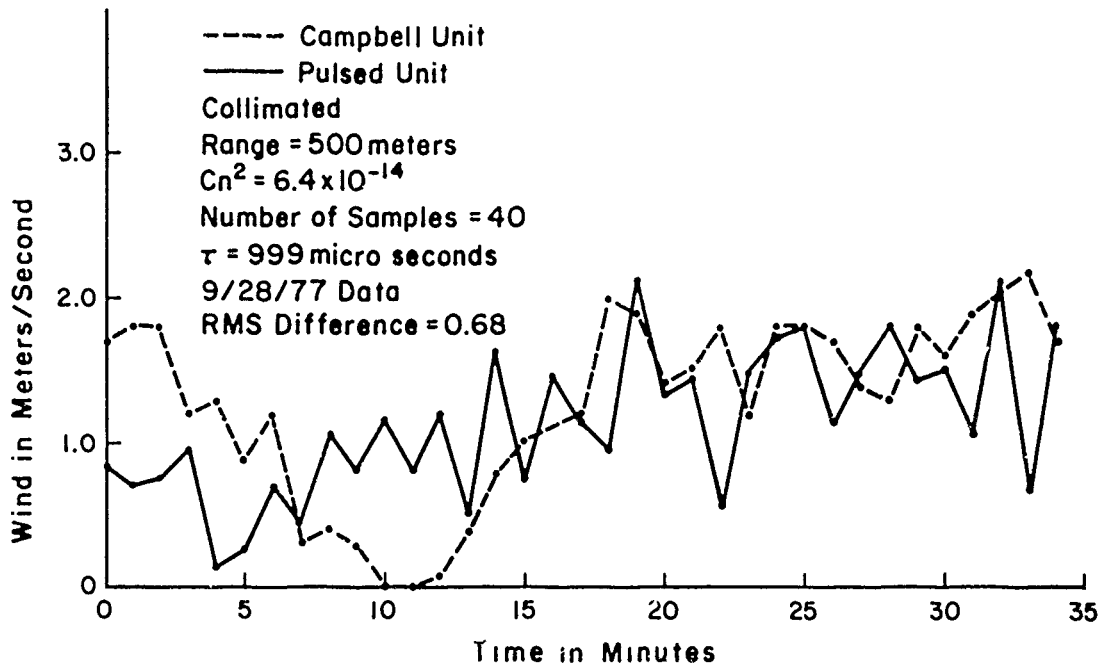

Figure 12. Crosswind, $C_n^2 = 6.4 \times 10^{-14}$.

Table 5. Crosswind Data $C_n^2 = 6.4 \times 10^{-14}$.

Oregon Graduate Center

Range = 500 meters
Time Between Pulses = 999 microseconds
Number of Samples = 40
$C_n^2 = 6.4 \times 10^{-14}$
Collimated Beam

Campbell Unit	Slope	Pulsed*
1.7	62	0.85
1.8	53	0.72
1.8	58	0.79
1.4	70	0.96
1.3	12	0.16
0.9	21	0.29
1.2	51	0.70
0.3	35	0.48
0.4	79	1.08
0.3	60	0.82
0	85	1.16
0	60	0.82
0.1	92	1.26
0.4	38	0.52
0.8	122	1.67
1.0	56	0.77
1.4	108	1.48
1.2	87	1.19
2.0	71	0.97
1.9	155	2.12
1.4	98	1.34
1.5	106	1.45
1.8	42	0.57
1.2	110	1.5
1.8	127	1.74
1.8	132	1.8
1.7	85	1.16
1.4	110	1.5
1.3	132	1.8
1.8	106	1.45
1.6	111	1.52
1.9	79	1.08
2.1	156	2.13
2.2	52	0.71
1.7	133	1.82

$\overline{W^2} = 2.039$ $\overline{S^2} = 8.45 \times 10^3$ $\overline{WS} = 1.155 \times 10^2$
RMS Difference = 0.68 m/second *Using Calibration Constant = 0.01367

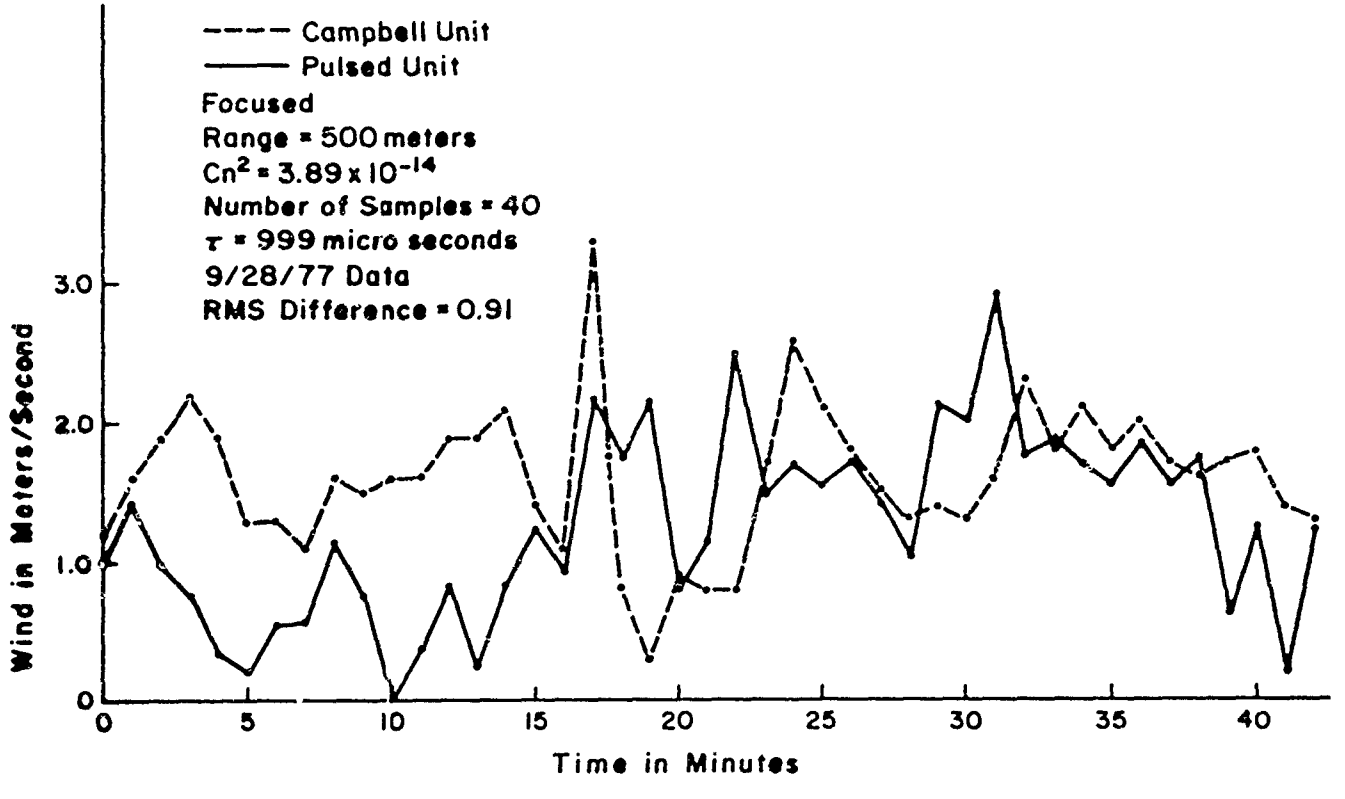

Figure 13. Crosswind, $C_n^2 = 3.89 \times 10^{-14}$.

Table 6. Crosswind data, $C_n^2 = 3.89 \times 10^{-14}$.

Oregon Graduate Center

Range = 500 meters
Time Between Pulses = 999 microseconds
Number of Samples = 40
$C_n^2 = 3.89 \times 10^{-14}$
Focused Beam

Campbell unit	Propellor anemometer	Slope	Pulsed 1*	Pulsed 2**
1.2	1.9	63	1.03	1.04
1.6	1.5	87	1.43	1.43
1.9	3.2	59	0.97	0.97
2.4	0	45	0.74	0.74
1.9	0	20	0.33	0.33
1.3	0	13	0.21	0.21
1.3	0.3	35	0.57	0.58
1.1	0	36	0.59	0.59
1.6	0	69	1.13	1.13
1.5	0.2	44	0.72	0.72
1.5	1.5	1	0	0
1.6	1.6	23	0.38	0.38
1.9	0.2	50	0.82	0.82
1.9	0.2	16	0.26	0.26
2.1	1.0	52	0.85	0.85
1.4	0.7	75	1.23	1.23
1.1	0.1	57	0.93	0.94
3.3	1.4	133	2.18	2.19
0.8	1.6	106	1.74	1.74
0.3	1.8	132	2.16	2.17
0.9	1.1	48	0.79	0.79
0.8	0	70	1.15	1.15
0.8	0	152	2.49	2.50
1.7	0.1	90	1.47	1.48
2.6	5.2	104	1.70	1.71
2.1	3.6	95	1.56	1.56
1.8	2.8	111	1.82	1.82
1.5	1.7	87	1.42	143
1.3	0.7	63	1.03	1.04
1.4	1.1	132	2.16	2.17
1.3	0	123	2.02	2.02
1.6	1.4	178	2.29	2.93
2.3	1.2	106	1.74	1.74
1.8	3.7	115	1.88	1.89
2.1	3.5	103	1.69	1.69
1.8	3.2	96	1.57	1.58

Table 6. Crosswind data, $C_n^2 = 3.89 \times 10^{-14}$.

Campbell unit	Propellor anemometer	Slope	Pulsed 1*	Pulsed 2**
2.0	3.3	114	1.87	1.87
1.7	3.2	96	1.57	1.58
1.6	2.7	106	1.74	1.74
1.7	0.4	38	0.62	0.62
1.8	0.2	78	1.28	1.28
1.4	0.4	14	0.23	0.23
1.3	0.9	75	1.23	1.23

*Comparison to Campbell Unit

$\overline{W^2} = 2.857$

$\overline{S^2} = 7.569 \times 10^3$

$\overline{WS} = 1.24 \times 10^2$

Calibration Constant = 0.01638

RMS Difference = 0.91

**Comparison to Propellor Anemometer

$\overline{W^2} = 3.503$

$\overline{S^2} = 7.569 \times 10^3$

$\overline{WS} = 1.244 \times 10^2$

Calibration Constant = 0.01644

RMS Difference = 1.232

gusty wind conditions. The column labeled 'slope' in the tables is the slope of the time delayed covariance function at zero time delay and is proportional to the path averaged crosswind.

For each data set, a calibration constant was calculated from the data such that the mean square error was a minimum. This constant was then used to calculate the pulsed system crosswind and the RMS error from the slope and in situ data.

In studying the results, it is apparent in some of the figures, particularly the first part of figures 12 and 13, that there are periods when the pulsed system and the Campbell unit do not track very well. During these periods the system generally reads low. We believe that this is caused by the two transmitter beams wandering in and out of alignment. It shows up to a lesser degree at higher turbulence levels which together with the low readings tends to support this conclusion.

During the focused beam measurements shown in figure 11, a single propellor anemometer was used in addition to the Campbell unit. It gives a single point wind reading and yields some insight into the degree of fluctuation of wind at a single point along the path. It is interesting to note that using the single propellor anemometer for the in situ data yielded the same calibration constant as using the Campbell unit for the in situ data.

One of the data sets was taken with the transmitter beams collimated rather than focused (figure 12). No substantial difference in performance was noted between the focused and collimated cases. However, there are two reasons to believe that better performance will be achieved with a focused transmitter: (1) the low turbulence limit of operation is determined by the relative scale sizes produced by the speckle and by the atmosphere and their relative scintillation strengths. Since for a focused transmitter the speckle scale size is equal to the transmitter size, $\sqrt{L/k}$, will dominate at the ranges of interest until the atmospheric scintillation strength is reduced below the speckle value. The speckle scale size from a collimated 3-inch beam is much smaller than the beam size; and, consequently, it is felt that the speckle would begin to dominate at a higher turbulence level than with a focused beam. In addition, the larger spot size on the target reduces the atmospheric scintillation strength. There may however be a trade off involving beam size that will allow collimated beam performance to very nearly match the focused beam performance. The use of a collimated beam is desirable from the standpoint that it would simplify system design. (2) There is a possibility that structure on the target may affect system performance. By using a focused beam, the spot size is determined primarily by the atmosphere most of the time. Consequently, any structure on the target (within the spot) will not be observed by the receiver and therefore should not have any effect on system performance. There may of course be a collimated beam size that accomplishes this same result.

CW EXPERIMENTAL WORK

Our cw experimental system (refs. 18,19) was used to collect data on the time delayed statistics. Specifically, the autocorrelation function and the time delayed covariance function were measured, and good qualitative agreement with the theory was obtained.

Measured autocorrelation functions for two wind speeds are shown in figures 14 and 15. The shape of the curves is consistent with theory; and as the wind speed increases, the correlation for a given time delay decreases as it should.

Figures 16 through 22 show measured time delayed covariance functions for both north and south winds. The shape is consistent with theory, and the peaks are on opposite sides of zero time delay for opposing wind directions, which yields a positive slope for a south wind and a negative slope for a north wind. The slope data and cross-wind calibration constant for each of the curves is shown in table 7. The measured slope at zero time delay is reasonably consistent with that measured by the pulsed system.

Good quantitative results are difficult to obtain for the time delayed statistics because the wind is not uniform along the path and generally fluctuates considerably with time. Consequently, it takes considerable time and effort to obtain good data.

In addition, more data was collected for the normalized variance of the intensity. It is shown in figure 23 along with a complete theoretical curve including the transition from low to saturated turbulence. The formulation for the theoretical curve was developing during the contract period and is contained in the next section.

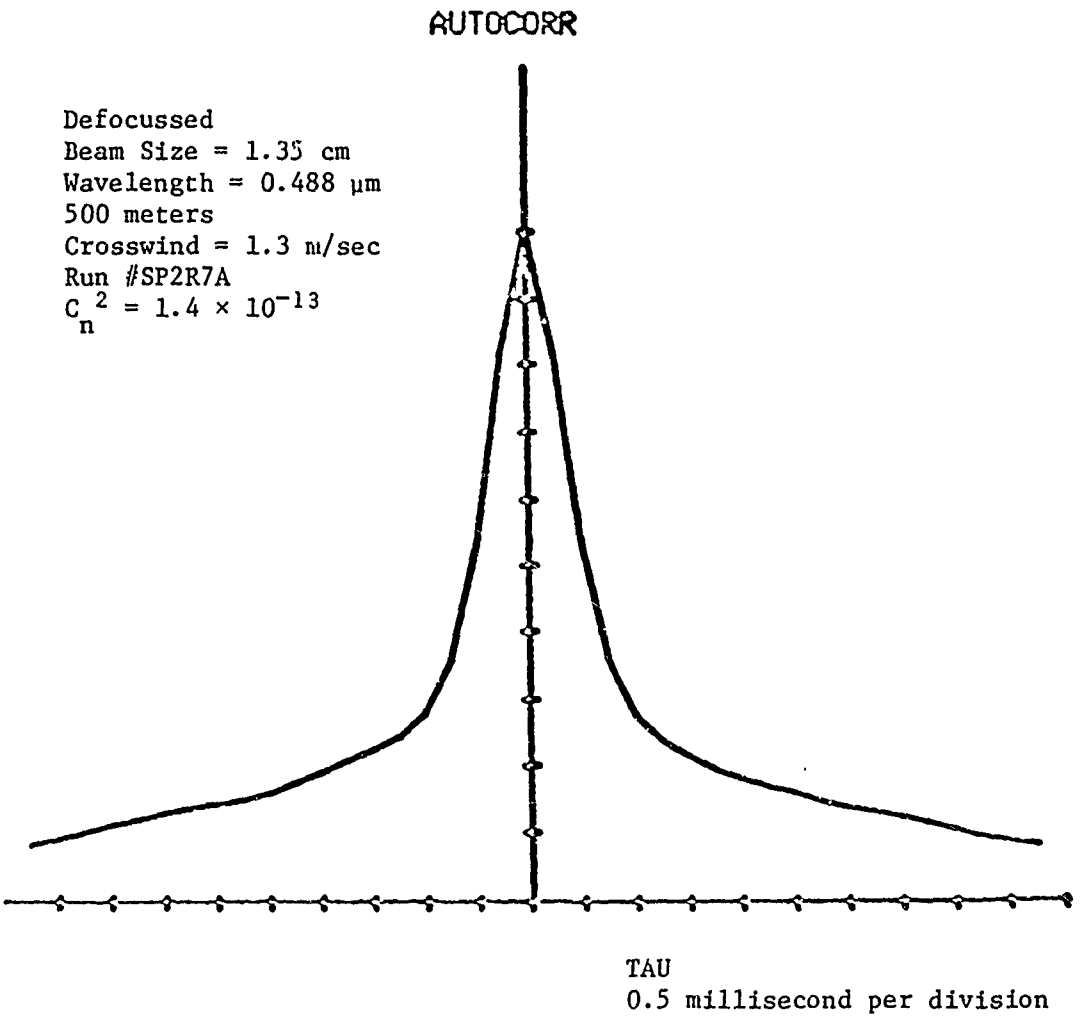

Figure 14. Autocorrelation function,
1.3 meters/second crosswind.

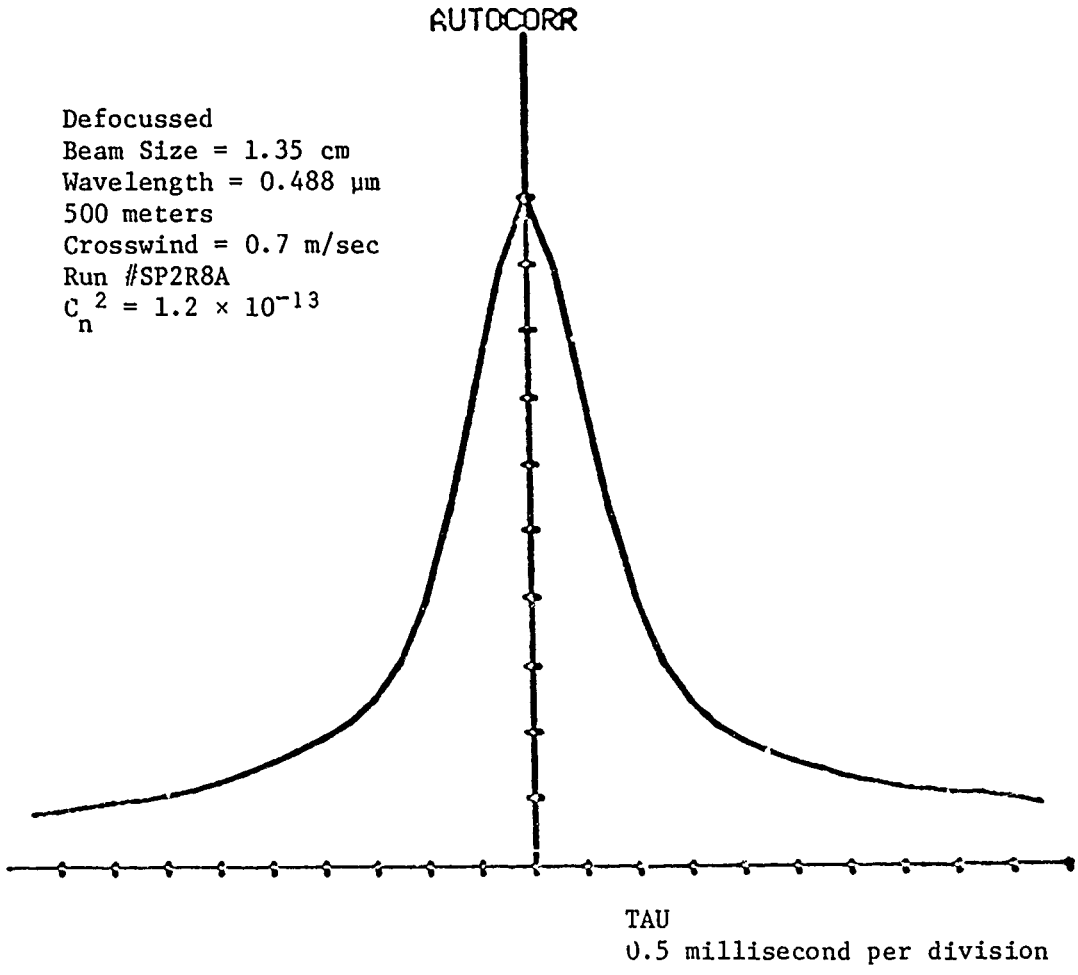

Figure 15. Autocorrelation function,
0.7 meter/second crosswind.

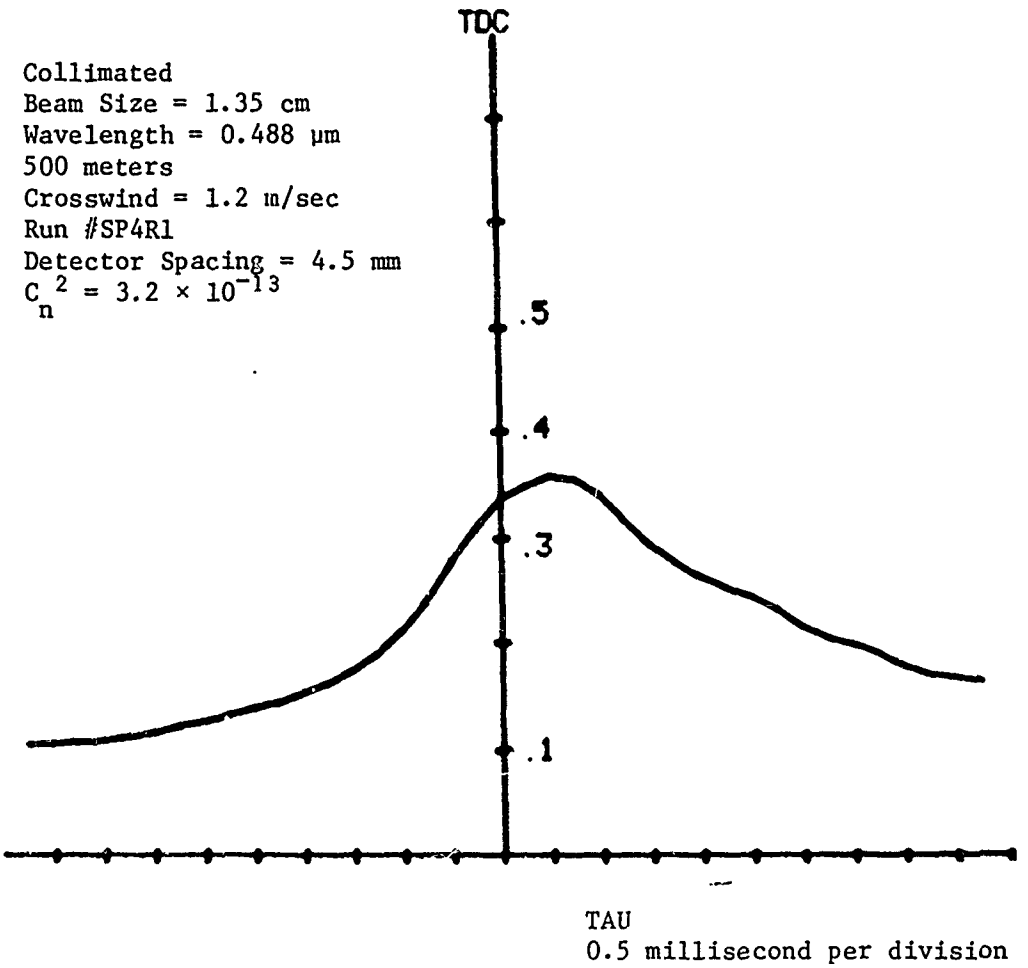

Figure 16. Time delayed covariance function, 1.2 meters per second south wind.

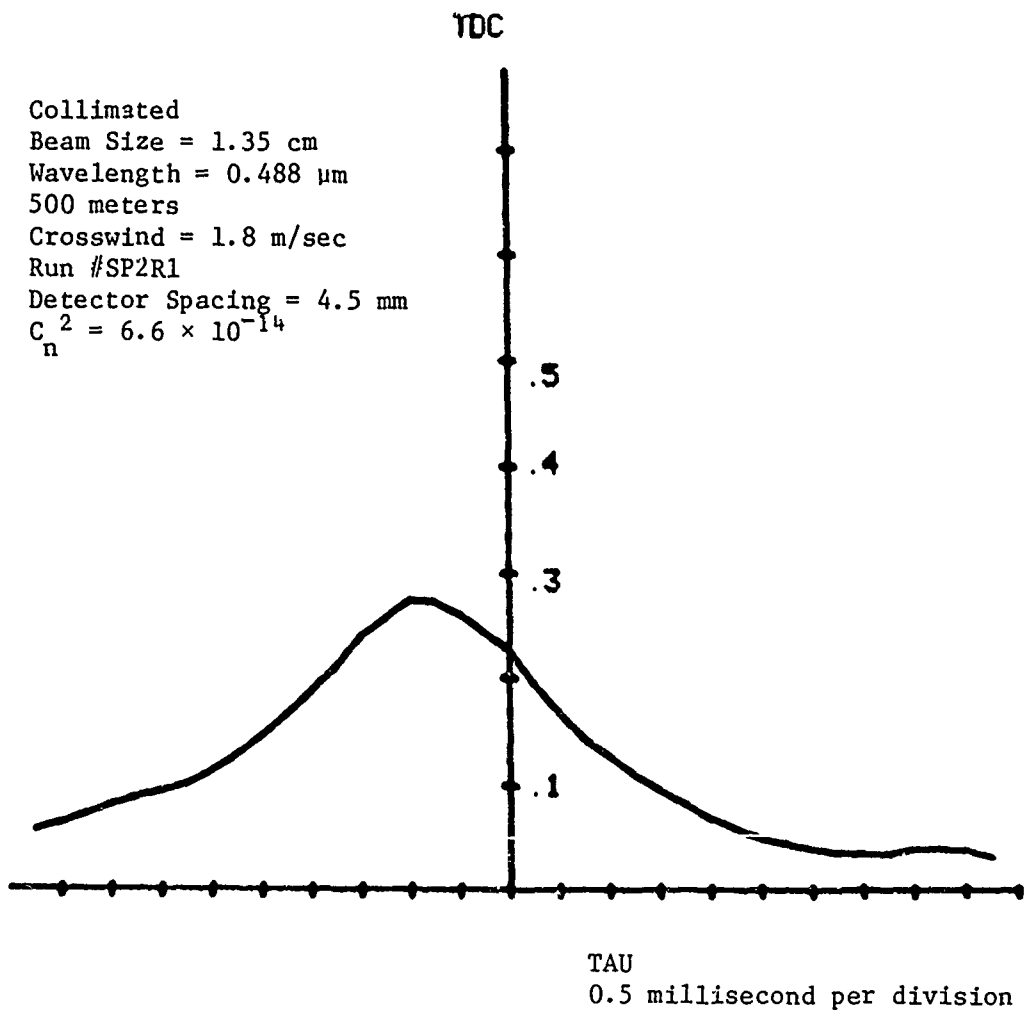

Figure 17. Time delayed covariance function, 1.8 meters per second north wind.

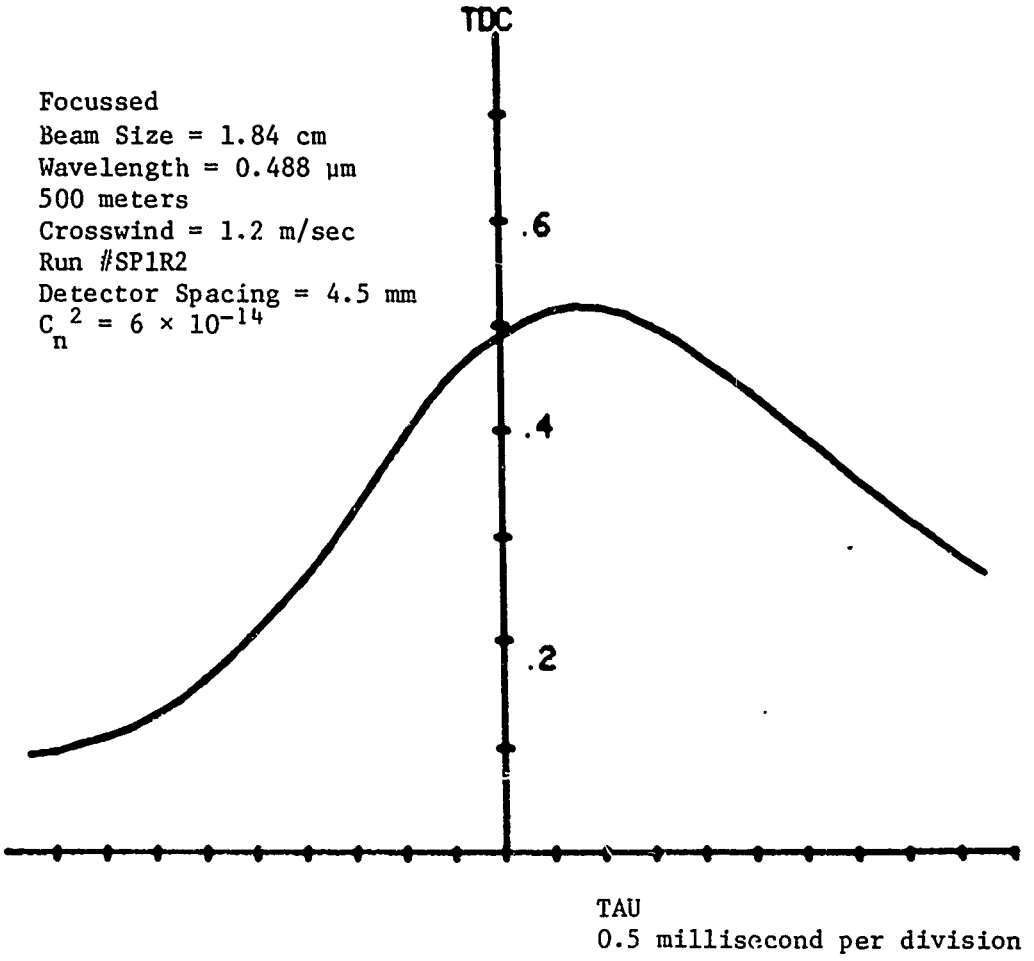

Figure 18. Time delayed covariance function, 1.2 meters per second south wind.

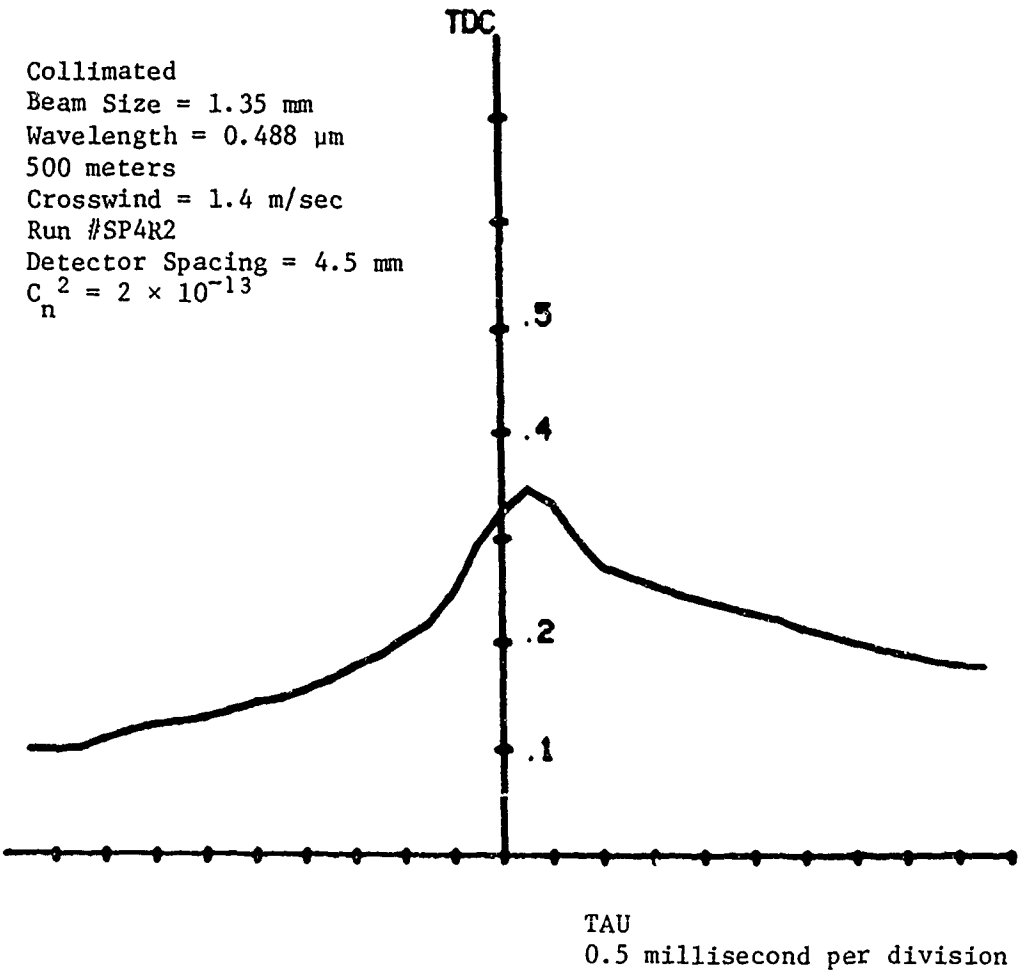

Figure 19. Time delayed covariance function, 1.4 meters per second south wind.

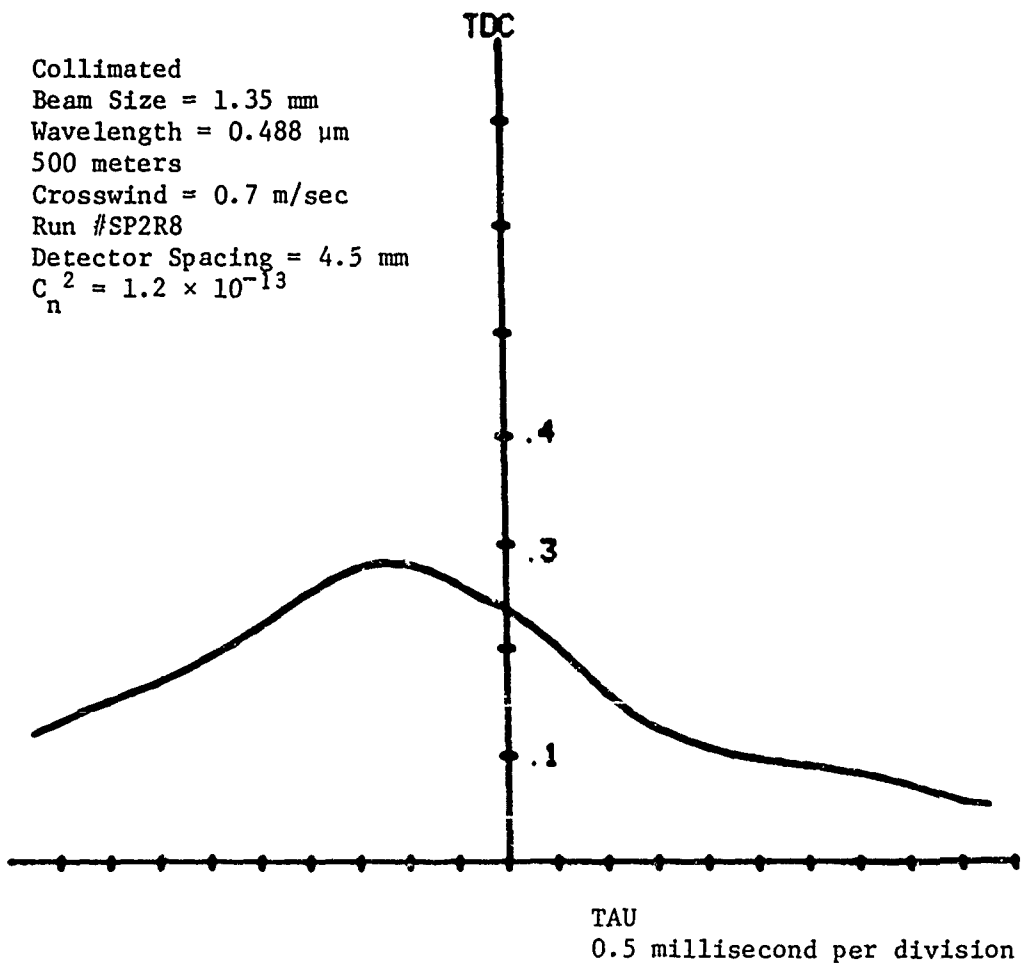

Figure 20. Time delayed covariance function, 0.7 meter per second north wind.

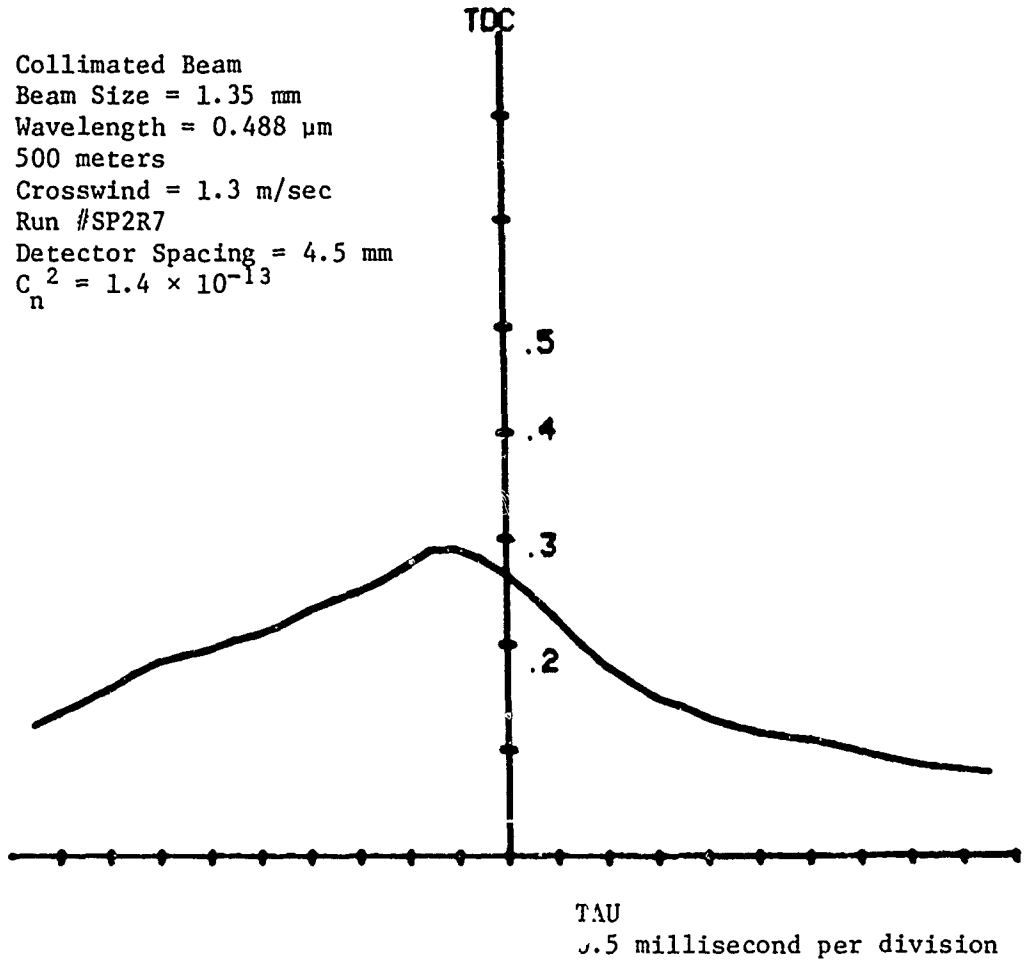

Figure 21. Time delayed covariance function, 1.3 meters per second north wind.

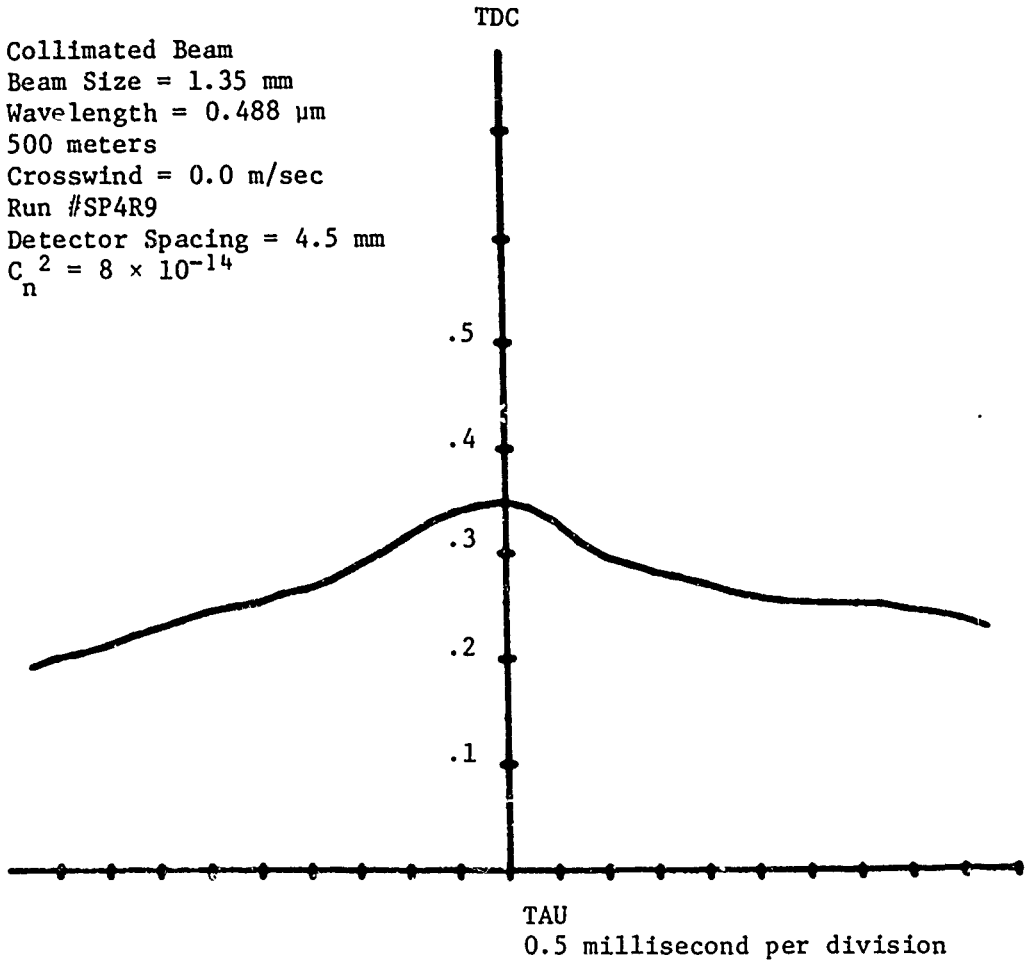

Figure 22. Time delayed covariance function, 0 meters per second wind.

Table 7. Slope data, τ = 1 millisecond.

F or C	Run #	Slope	Crosswind	Slope/Crosswind = Cal. Const.
Collimated	SP4R1	+ 80	1.2 S	0.015
Collimated	SP2R1	- 91.5	1.8 N	0.0197
Focussed	SP1R2	62	1.2 S	0.019
Collimated	SP4R2	87	1.4 S	0.016
Collimated	SP2R8	- 61	0.7 N	0.012
Collimated	SP2R7	- 66	1.3 N	0.0198

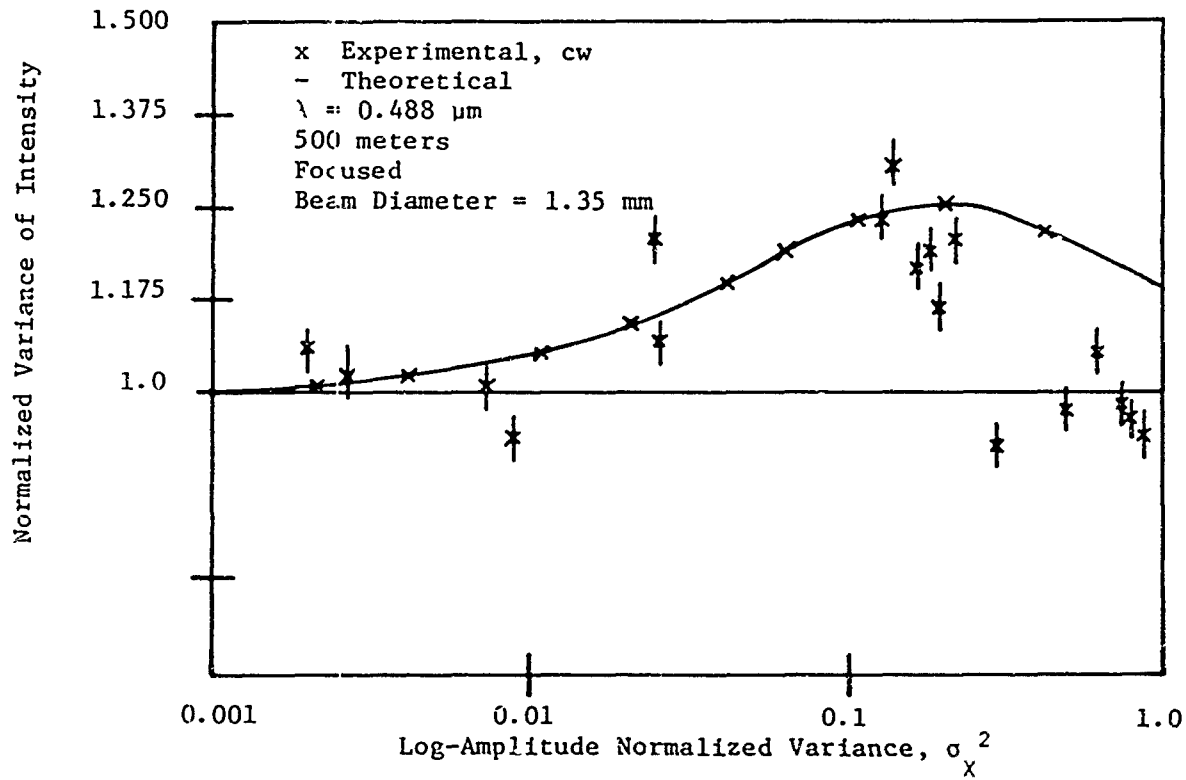

Figure 23. Normalized variance of intensity versus σ_x^2.

ANALYSIS AND NUMERICAL WORK

The theoretical formulations (ref 18) for the statistics of the received intensity were developed in terms of the wave structure function D_ψ and log-amplitude covariance function C_χ. A direct calculation of C_χ for use in the theoretical formulations proved to be too slow to be useful. Consequently, an algorithm for efficiently generating C_χ has been developed. A formulation for the log-amplitude covariance function good for all levels of turbulence is given by (ref. 20)

$$C_\chi(\rho,\sigma_T^2) = 2.95\,\sigma_T^2 \int_0^1 du\,[u(1-u)]^{5/6} \int_0^\infty dy\,\frac{\sin^2 y}{y^{11/6}} \times \exp\left\{-\sigma_T^2\,[u(1-u)]^{5/6}\,f(y)\right\} J_0\left[\left(\frac{4\pi y u}{1-u}\right)^{1/2}\frac{\rho}{\sqrt{\lambda L}}\right] \tag{1}$$

where

$$\sigma_T^2 = .124\,k^{7/6}\,L^{11/6}\,C_n^2 \tag{2}$$

$$f(y) = 7.02\,y^{5/6}\int_{.7y}^\infty dx\,x^{-8/3}\,[1 - J_0(x)] \tag{3}$$

and

J_0 is the zero-order Bessel function. We first consider the exponential factor f(y), and define the function g(q) as

$$g(q) = \int_q^\infty dx\,x^{-8/3}\,[1 - J_0(x)]\,dx \tag{4}$$

It can be integrated by parts to yield

$$\begin{aligned} g(q) &= \frac{3}{5}\,q^{-5/3}\,[1 - J_0(q)] + \frac{3}{5}\int_q^\infty dx\,x^{-5/3}\,J_1(x) \\ &= \frac{3}{5}\,q^{-5/3}\,[1 - J_0(q)] + \frac{3}{5}\int_0^\infty dx\,x^{-5/3}\,J_1(x) \\ &\qquad - \frac{3}{5}\int_0^q dx\,x^{-5/3}\,J_1(x) \end{aligned} \tag{5}$$

We can make use of the integral formula

$$\int_0^\infty dx\,x^{-5/3}\,J_1(x) = 2^{-5/3}\,\frac{\Gamma(1/6)}{\Gamma(11/6)}$$

and the integral representation

$$J_1(bu) = \frac{2bu}{\pi} \int_0^1 dt\sqrt{1 - t^2} \cos(but)$$

to reduce (5) to

$$g(q) = \frac{3}{5} q^{-5/3} [1 - J_o(q)] + \frac{3}{5} 2^{-5/3} \frac{\Gamma(1/6)}{\Gamma(11/6)}$$

$$- \frac{6}{5\pi} \int_0^1 dt\sqrt{1 - t^2} \int_0^q dx\, x^{-2/3} \cos xt \qquad (6)$$

Now using the integral identity,

$$\int_0^q dx\, x^{\mu-1} \cos xt = \frac{q\mu}{2\mu} \left[{}_1F_1(\mu; \mu + 1; iqt) + {}_1F_1(\mu; \mu + 1; - iqt)\right] \qquad (7)$$

where ${}_1F_1$ is the confluent hypergeometric function we obtain

$$g(q) = \frac{3}{5}\left\{q^{-5/3} [1 - J_o(q)] + 1.863893834 - \frac{6}{\pi} q^{1/3} \int_0^1 dt\, \sqrt{1 - t^2} \left[1 - \frac{1}{7} \frac{q^2t^2}{2!} + \frac{1}{13} \frac{q^4t^4}{4!} - \frac{1}{19} \frac{q^6t^6}{6!} + \frac{1}{25} \frac{q^8t^8}{8!} - \ldots.\right]\right\} \qquad (8)$$

The integration over t can now be evaluated by making use of the integral identity

$$\int_0^1 dt\, t^{2n} \sqrt{1 - t^2} = \frac{1}{2} \frac{\Gamma\left(\frac{2n + 1}{2}\right)\Gamma(3/2)}{\Gamma(n + 2)} \qquad (9)$$

Performing the integration Eq.(8) becomes

$$g(q) = 3\left\{.37278 - \frac{q^{1/3}}{4} + \frac{q^{7/3}}{448} - \frac{q^{13/3}}{29952} + \frac{q^{19/3}}{2801664} - \frac{q^{25/3}}{368640000}\right\} + \Delta(q) \qquad (10)$$

where $|\Delta(q)| < .00041$ for $q \leq \frac{3}{2}\pi$.

For large values of q we can obtain an asymptotic series by using the asymptotic expansion for $J_o(x)$ in Eq.(4). It becomes

$$g(q) \sim \frac{3}{5} q^{-5/3} - \frac{1}{\sqrt{\pi}} \int_q^\infty dx\, x^{-19/6} \cos x$$

$$- \frac{1}{\sqrt{\pi}} \int_q^\infty dx\, x^{-19/6} \sin x \qquad (11)$$

Using the integral identity

$$\int_0^1 x^{\mu-1} \sin(ax) = \frac{-i}{2\mu} \left[{}_1F_1(\mu;\, \mu + 1;\, ia) - {}_1F_1(\mu;\, \mu + 1;\, -ia) \right] \qquad (12)$$

Eq.(11) becomes

$$g(q) \sim \frac{3}{5} q^{-5/3} - \frac{1}{2\sqrt{\pi}} \left[e^{i\frac{13\pi}{12}} \Gamma\left(-\frac{13}{6},\, iq\right) + e^{-i\frac{13\pi}{12}} \Gamma\left(-\frac{13}{6},\, -iq\right) \right]$$

$$- \frac{1}{2\sqrt{\pi}} \left[e^{i\frac{13\pi}{12}} \Gamma\left(-\frac{13}{6},\, iq\right) - e^{-i\frac{13\pi}{12}} \Gamma\left(-\frac{13}{6},\, -iq\right) \right] \qquad (13)$$

where $\Gamma(a,b)$ is the incomplete gamma function. Equation (13) can be rewritten as

$$g(q) \approx \frac{3}{5} q^{-5/3} - \frac{(1+i)}{2\sqrt{\pi}} e^{i\frac{13\pi}{12} - iq} U\left(\frac{19}{6}, \frac{19}{6}, iq\right)$$

$$- \frac{1-i}{2\sqrt{\pi}} e^{-i\frac{13\pi}{12} + iq} U\left(\frac{19}{6}, \frac{19}{6}, -iq\right)$$

$$\approx \frac{3}{5} q^{-5/3} - \sqrt{\frac{2}{\pi}} \cos\left(q + \frac{\pi}{4}\right) \left[q^{-19/6} - \frac{19}{6} \cdot \frac{25}{6} q^{-31/6} \right.$$

$$\left. + \frac{19}{6} \cdot \frac{25}{6} \cdot \frac{31}{6} \cdot \frac{37}{6} q^{-43/6} - \ldots \right]$$

$$- \sqrt{\frac{2}{\pi}} \sin\left(q + \frac{\pi}{4}\right) \left[\frac{19}{6} q^{-25/6} - \frac{19}{6} \cdot \frac{25}{6} \cdot \frac{31}{6} q^{-37/6} \right.$$

$$\left. + \frac{19}{6} \cdot \frac{25}{6} \cdot \frac{31}{6} \cdot \frac{37}{6} \cdot \frac{43}{6} q^{-49/6} - \ldots \right] \qquad (14)$$

where U is confluent hypergeometric function of the second kind. Using Eq.(14) in (13) yields

$$f(y) = 9.45\ (.7y)^{5/6}\ g(.7y) \tag{15}$$

By using (15) in the expression for C_χ given by Eq.(1) and performing the u and y integrations using Gaussian quadrature, numerical values of C_χ can be efficiently obtained.

In addition to the above work, some additional analytic work was accomplished on the n^{th} order mutual coherence function first formulated in reference 18. The work has been published (ref. 21); and so, it will not be repeated in this report.

REFERENCES

1. D. L. Walters, "Crosswind Weighting Functions for Direct-Fire Projectiles," U.S. Army Electronics Command, Research and Development Report ECOM-5570, Atmospheric Sciences Laboratory, White Sands Missile Range, New Mexico 88002, August 1975.

2. R. S. Lawrence, G. R. Ochs, and S. F. Clifford, "The Use of Scintillations to Measure Average Wind Across a Light Beam," Appl. Opt., 11, 239, 1972.

3. G. R. Ochs, G. F. Miller, "Pattern Velocity Computers - Two Types Developed for Wind Velocity Measurements by Optical Means," Rev. of Sci. Instrum., 43, 879, 1974.

4. T. H. Pries, E. T. Young, "Evaluation of a Laser Crosswind System," U.S. Army Electronics Command Research and Development Technical Report, ECOM-5546.

5. G. R. Ochs, S. F. Clifford, and T. I. Wang, "A Feasibility Study of an Optical Crosswind Monitor," NOAA Technical Memorandum WPL-10, 1973.

6. S. F. Clifford, G. R. Ochs and Ting-i Wang, "Theoretical Analysis and Experimental Evaluation of a Prototype Passive Sensor to Measure Crosswinds," NOAA Technical Report ERL 312-WPL 35, September 1974.

7. Ting-i Wang, S. F. Clifford and G. R. Ochs, "Wind and Refractive - Turbulence Sensing Using Crossed Laser Beams," Appl. Opt., 13, 2602, 1974.

8. S. F. Clifford, G. R. Ochs and Ting-i Wang, "Optical Wind Sensing by Observing the Scintillations of a Random Scene," Appl. Opt., 14, 2844, 1975.

9. G. R. Ochs, S. F. Clifford, and Ting-i Wang, "Laser Wind Sensing: the Effects of Saturation of Scintillation," Appl. Opt., 15, 403, 1976.

10. J. Smith, "Folded Path Weighting Function for a High Frequency Spherical Wave," J. Opt. Soc. Am., 63, 1095, 1973.

11. J. Smith, T. H. Pries, K. J. Skipka, and M. A. Hamiter, "High Frequency Plane-Wave Filter Function for a Folded Path," J. Opt. Soc. Am., 62, 1183, 1972.

12. I. I. Goldberg, "Considerations of Automatic Tracker Application in Combat Vehicles," Department of the Army, Frankford Arsenal Memorandum Report M68-37-1, Philadelphia, Pa. 19137, November 1968.

13. J. R. Kerr, "Microwave-Bandwidth Optical Systems," Proc. IEEE, 55, 1686, 1967.

14. J. F. Holmes and J. R. Kerr, "Experimental Pulsed Laser, Remote Crosswind Measurement System -- Feasibility Study and Design," U.S. Army Electronics Command, Research and Development Technical Report ECOM 74-0094-1, Atmospheric Sciences Laboratory, U.S. Army Electronics Command, White Sands Missile Range, New Mexico 88002, July 1974.

15. J. F. Holmes, J. R. Kerr, et al., "Experimental Pulsed Laser, Remote Crosswind Measurement System -- Feasibility Study and Design (Part II)," U.S. Army Electronics Command, Research and Development Technical Report ECOM75-1, Atmospheric Sciences Laboratory, U.S. Army Electronics Command, White Sands Missile Range, New Mexico 88002, January 1975.

16. J. F. Holmes, J. R. Kerr, et al., "Experimental Pulsed Laser, Remote Crosswind Measurement System -- Feasibility Study and Design (Part III)," U.S. Army Electronics Command, Research and Development Technical Report ECOM75-1, Atmospheric Sciences Laboratory, U.S. Army Electronics Command, White Sands Missile Range, New Mexico 88002, September 1975.

17. M. H. Lee, J. Fred Holmes, and J. R. Kerr, "Statistics of Speckle Propagation Through the Turbulent Atmosphere," J. Opt. Soc. Am., 66, 1164, 1976.

18. J. F. Holmes, J. R. Kerr, et al., "Experimental Pulsed Laser, Remote Crosswind Measurement System -- Feasibility Study and Design (Part IV)," U.S. Army Armament Command, Research and Development Technical Report FA-TA-76065, Frankford Arsenal, Philadelphia, Pa. 19137, November 1976.

19. Philip A. Pincus, Michael E. Fossey, J. F. Holmes, J. Richard Kerr, "Speckle Propagation Through Turbulence - Experimental," J. Opt. Soc. Am., 68, 760, 1978.

20. S. F. Clifford and H. T. Yura, "Equivalence of Two Theories of Strong Optical Scintillation," J. Opt. Soc. Am., 64, 1641, 1974.

21. M. H. Lee, J. F. Holmes and J. R. Kerr, "Generalized Spherical Wave Mutual Coherence Function," J. Opt. Soc. Am., 67, 1279, 1977.

DISTRIBUTION LIST

Director
Defense Advanced Research Projects Agency
ATTN: Dir. Tactical Technology Office
Mr. G. H. Sigman, Jr.
1400 Wilson Blvd.
Arlington, VA 22209

US ARMY RESEARCH OFFICE
ATTN: DRXRO-GS - Dr. A. Dodd
P.O. Box 12211
Research Triangle Park, NC 27709

Defense Documentation Center (12)
Cameron Station
Alexandria, VA 22314

COMMANDER
US ARMY ARRADCOM
ATTN: DRDAR-CG
DRDAR-SC - Col. A. Larkins
DRDAR-SC - Dr. D. A. Gyorog
DRDAR-SCP
DRDAR-SCF - Mr. L. Berman
DRDAR-SCF-I - Mr. J. Lehman (2)
DRDAR-SCF-IE - Mr. J. Heater (10)
DRDAR-SCF-IO - Dr. J. Zavada
DRDAR-SCF-A - Mr. G. Staton
DRDAR-SCF-AV - Mr. E. DelCoco
DRDAR-SCF-AV - Mr. K. Pfleger
DRDAR-SCF-AV - Mr. R. Volz
DRDAR-SCF-AI - Dr. J. Kervorkian
DRDAR-SCF-D - Mr. W. Ryba
DRDAR-SCF-DA - Mr. J. Spangler
DRDAR-SCF-DD - Mr. S. Goodman
DRCPM - ADG - E - Mr. R. Seamands
DRCPM - CAWS - GP - Mr. G. Waldron
DRDAR-TSS (5)
DRDAR-SCS-E - Mr. D. Brandt
Dover, NJ 07801

COMMANDER
US ARMY ARRADCOM
Ballistic Research Laboratory
ATTN: DRDAR - BLG - Dr. S. Wolf
DRDAR - BLB - Mr. A. LaGrange
Aberdeen Proving Ground, MD 21005

COMMANDER
US ARMY ARRADCOM
Chemical Systems Laboratory
ATTN: DRDAR-CLB-PS - Dr. E. Stuebing
Aberdeen Proving Ground, MD 21010

COMMANDER
US ARMY AVRADCOM
ATTN: DRDAV-N
Mr. D. Weller
St. Louis, MO 63166

COMMANDER
US ARMY ERADCOM
NV & EO Laboratory
ATTN: DELNV-L - Dr. R. Buser
DRSEL-NVDX - Mr. J. Johnson
DELNV-I - Mr. R. Moulton
Ft. Belvoir, VA 22060

COMMANDER
US ARMY ERADCOM
Atmospheric Sciences Laboratory
White Sands Missile Range
ATTN: DELAS-AS-M - Dr. D. Walters
DELAS-AS-P - Mr. T. Pries
DELAS-BL-SK - Dr. R. Gomez
White Sands, NM 88002

COMMANDER
US ARMY TARADCOM
ATTN: DRDTA-RDAF - Mr. J. Bush
Warren, MI 48090

DIRECTOR
US ARMY TRADOC SYSTEMS
Analysis Activity
ATTN: ATAA-SL (Tech Lib)
White Sands Missile Range, NM 88002

Technical Library
ATTN: DRDAR-CLJ-L
Aberdeen Proving Ground, MD 21005

Technical Library
ATTN: DRDAR-TSB-S
Aberdeen Proving Ground, MD 21010

Technical Library
ATTN: DRDAR-LCB-TL
Benet Weapons Laboratory
Watervliet, NY 12189